Substrate traits govern the assembly and spatial organization of microbial community engaged in metabolic division of labor

Miaoxiao Wang
Peking University
Xiaoli Chen
Peking University
Yong Nie
Peking University https://orcid.org/0000-0002-5940-1218
Xiao-Lei Wu (xiaolei_wu@pku.edu.cn)
Peking University https://orcid.org/0000-0002-9897-6903

Article

Keywords: metabolic division of labor, microbial community, spatial organization

Posted Date: December 2nd, 2020

DOI: https://doi.org/10.21203/rs.3.rs-110849/v1

Full title: Substrate traits govern the assembly and spatial organization of microbial community engaged in metabolic division of labor

Running title: Substrate traits affect microbial division of labor

Miaoxiao Wang[1], Xiaoli Chen[1, 2], Yong Nie[1#] and Xiao-Lei Wu[1, 2, 3#]

[1] College of Engineering, Peking University, Beijing 100871, China

[2] Institute of Ocean Research, Peking University, Beijing 100871, China

[3] Institute of Ecology, Peking University, Beijing 100871, China

[#]Corresponding author: Research Scientist, College of Engineering, Peking University.

Tel: +86 10-62759047; Fax: +86 10-62759047; E-mail: nieyong@pku.edu.cn

[#]Corresponding author: Professor, College of Engineering, Peking University.

Tel: +86 10-62759047; Fax: +86 10-62759047; E-mail: xiaolei_wu@pku.edu.cn

Abstract

Metabolic division of labor (MDOL) is widespread in nature, whereby a complex metabolic pathway is shared between different strains within a community for mutual benefit. However, little is known about how communities engaged in MDOL assemble and spatially organize. We hypothesized that when degradation of an organic compound is carried out via MDOL, substrate concentration and its toxicity modulate the benefit allocation between the two microbial populations, thus governing the assembly of this community. We tested this hypothesis by combining individual-based simulations with pattern formation assays using a synthetic microbial community. We found that while the frequency of the first population increases with an increase in substrate concentration, this increase is capped with an upper bound determined by the biotoxicity of the substrate. In addition, our model showed that substrate concentration and its toxicity affect levels of intermixing between strains. These predictions were quantitatively verified using an engineered system composed of two strains degrading salicylate through MDOL. Our results demonstrate that the structure of the microbial communities can be quantitatively predicted from simple environmental factors, such as substrate concentration and its toxicity, which provides novel perspectives on understanding the assembly of natural communities, as well as insights into how to manage artificial microbial systems.

Introduction

In natural environments, microorganisms rarely live autonomously, but interact with other individuals to form complex communities, in which they secrete a variety of toxins to compete with each other, or share metabolites to mutually benefit their survival. Among a variety of modes of microbial interaction, metabolic division of labor (MDOL) is one of the most widespread phenomena, where distinct populations perform different but complementary steps of the same metabolic pathway[1-4]. MDOL controls numerous ecologically and environmentally important biochemical processes. For example, the nitrification pathway is often operated by the collaboration between two populations, in which the first group oxidizes ammonia to nitrite, before being converted to nitrate by another bacterial group[5]. Similarly, during the Deepwater Horizon oil spill Gulf of Mexico (2010), complete degradation of polycyclic aromatic hydrocarbons (PAHs) required the partitioning of key pathway steps into several bacterial groups[6]. Since each population only contains a subset of genetic components required for the overall pathway, MDOL is thought to be a key evolutionary strategy to reduce metabolic burden of each individual[7,8]. In addition, bacteria have been found to use this strategy to reduce the inter-enzyme competition and the inhibitory effects of intermediates, thus improving the systematic metabolic efficiency[9]. Furthermore, MDOL vastly enhances functional differentiation of microbial communities, contributing to genetic diversity in complex ecosystem[7,8]. Nevertheless, how microbial communities engaged in MDOL assemble remains poorly understood. Understanding the assembly rules of communities engaged in MDOL is fundamental for better

evaluating their contribution to the natural biochemical cycle.

One important aspect of microbial metabolism implemented by MDOL is the degradation of a variety of organic compounds, including PAHs, lignin or chitin. Bacterial degradation of these complex substrates is usually mediated by long metabolic pathways via a number of intermediates. While these pathways often remain intact within one population, they are frequently found segregated across different members within a community, whereby the intermediates are being secreted by one species, before being utilized as substrate by another species for further processing along the same pathway. Typical examples include syringate degradation via sequential cross-feeding between *Acetobacterium woodii* and *Pelobacter acidigallici*[10], phenanthrene degradation between *Marinobacter* sp. N4 and other PAH-degrading microbes in marine environments[11], as well as atrazine degradation through MDOL within four bacterial species[12]. Nevertheless, all of these natural communities grow in the environments that may fluctuate over time and vary in space. For example, the concentration of the initial substrate, such as PAHs and other hydrocarbons, is highly fluctuating over time and different sites in the marine[13], soil[14] and wastewater[15] environments. It still remains poorly understood whether specific environmental factors, such as the traits of the substrate, affect the relative fitness of strains engaged in MDOL, and thus govern the assembly of these communities.

Moreover, microorganisms often live in spatially structured environments, forming well-organized biofilms[16,17]. Diverse interactions among species within these biofilms drive to intricate spatiotemporal dynamics, which in turn, affect the assembly and

productivity of such communities[17-20]. Particularly, communities engaged in MDOL commonly form specific patterns. For example, a number of studies have previously reported that anaerobic methanotrophic archaea at the surface of a deep seabed perform the first step of oxidation of methane, converting methane to hydrogen, before being transformed into bicarbonate by their bacterial partners[21-24]. These studies also found that such communities self-organize into microcolonies with different morphologies, such as mixed-type[21,25,26], mat-type[21,25], as well as shell-type[21,27,28]. In these colonies, the average distances between cells from different populations, i.e., the levels of intermixing, vary considerably, which appears to be correlated with the taxa of the archaea and bacteria[21]. Another recent study investigating how a well-defined community engaged in MDOL spatially self-organized on surface, suggested that MDOL generally favored strong intermixing between the two strains involved, and the levels of intermixing are also correlate with the degree of wetness at the surface[29]. Therefore, the levels of intermixing of different strains within MDOL communities appear to rely on abiotic conditions. Therefore, insights into the factors affecting the levels of intermixing among different strains is critical for a more detailed understanding of the rules governing community assembly in heterogeneous environments.

Here, we set out to investigate how MDOL drives assembly and spatial organization of microbial communities by combining mathematical modelling and experimental research using a synthetic microbial community. More specifically, we focused on the effect of substrate traits, that is, its initial concentration and its toxicity.

Results

The hypotheses of this study

We first proposed a hypothesis on how substrate concentration and its toxicity govern the assembly of microbial community engaged in MDOL, which is based on the feature of resource allocation among different members executing organic compounds degradation via MDOL. In these cases, the direct carbon sources, such as small organic acids or coenzyme A, to support bacterial growth, but these available nutrients are normally present as the final product of a pathway (Supplementary Figure 1). Therefore, the population performing the last steps can preferentially acquire and privatize these nutrients (which we henceforth call *product privatization*), thus acquiring the greater benefit, while other members have to collect nutrients released from this population (Figure 1A). We proposed a hypothesis based on this phenomenon: in an organic compound degradation community engaged in MDOL, the population executing the last steps of the pathway will dominate the community due to its privatization of the limited resources (we called this benefit *private benefit* below). This selfish population is analogous to a human worker responsible for the final step of an assembly line, who pockets the final product and rarely share profits with other workers. Thus, we named this final strain at the end of a MDOL-enabled pathway the 'Embezzler'. Following this hypothesis, we also derived two corollaries. Firstly, increasing concentration of the substrate improves the flux of the pathway, whereby more end product is released from the 'Embezzler' strain, in turn facilitating the growth of the other population (Figure 1B). Secondly, the presence of an initial substrate with a biotoxicity, which is frequently

observed during organic compound degradation, favors the population performing the first step, because it is capable of detoxifying the initial substrate by transforming the substrate to the intermediates (Figure 1C). In summary, in presence of the resource privatization by the 'Embezzler' population, concentration and toxicity of the substrate can be two key factors that govern the assembly of organic compound degradation community engaged in MDOL. The goal of this study is to test this prediction.

Individual-based modelling of spatial organization of MDOL community.

To test our hypothesis about Embezzler behavior, as well as the effects of substrate concentration and toxicity, we simulated the assembly and spatial organization of MDOL community by constructing an individual-based model. As summarized in Supplementary Figure 2, we considered the degradation of an organic substrate (S) into an intermediate metabolite (I) by one enzyme (E1), before being degraded to the final product (P) by a second enzyme (E2). We assumed that two strains carry out this pathway via MDOL, where the first strain only expresses E1, and the second only expresses E2. Initially, only S was supplied in the environment and evenly distributed across the entire habitat. Importantly, based on our hypothesis of how organic compounds are degraded in community engaged in MDOL, we assumed that, P, which was synthesized by the second strain, was the sole available resource for the growth of both strains, while neither S nor I can be directly used for growth. Therefore, the second strain possessed the advantage of preferentially acquiring the resource, while the first strain only obtained those growth-limiting resource that were secreted from the second strain. Therefore, the second strain behaved as an 'Embezzler'. Moreover, biotoxicity

150 of the substrate was imposed by adding a hyperbolic toxic term[30] to the growth function,
151 and the toxic strength was mediated by parameter *t*. As the first population detoxified
152 the toxic substrate, we named it 'Detoxifier'. Details about the model construction are
153 described in Supplementary Information S1.
154 We initiated each simulation by randomly scattering a 1:1 (200-cell) mixture of the two
155 cell types in a circle of 200-μm radius. When toxicity was not considered and substrate
156 concentration was low (e.g., $t = 0$ and $S = 5$ C-mmol/L), the model successfully
157 reproduced our hypothesis of 'Embezzler' behavior. In this case, 'Embezzler' cells
158 grew much faster than Detoxifier cells and occupied large majority of the space with a
159 relative fraction of 97.74% ± 0.04% (Figure 2A; Supplementary video 1).
160 We then tested the corollary 1 stating that substrate concentration mediates the assembly
161 of the community, by performing simulations with eight different initial substrate
162 concentration and without substrate toxicity. As shown in Figure 2, with the increase of
163 substrate concentration, the relative fraction of Detoxifier population increased and
164 gradually reached a steady frequency around 35% (Figure 2A and B; Supplementary
165 video 2). To test whether this shift occurred due to the increase concentration of the
166 final product released by the 'Embezzler' cells (i.e., corollary 1, Figure 1B), we
167 analyzed the intracellular and extracellular product concentration of the two
168 populations. Our analysis showed that with the increase of substrate input, the fraction
169 of final product released by the Embezzler population (that is, the ratio of extracellular
170 to intracellular concentration) increased (Supplementary Figure 3 A and B), so the
171 Detoxifier obtained more product from the environment, resulted in a higher

intracellular product concentration, which gradually approached that of the Embezzler (Supplementary Figure 3 A and C). Importantly, even if the substrate input was elevated to high levels (For example, $S = 40$ C-mmol/L), the intracellular product concentration of the Detoxifier never exceeded that of the Embezzler (Supplementary Figure 3 A and C). As a result, Embezzler cells maintained their growth advantage from privatizing end product. Together, these results showed that substrate concentration governs the assembly of community engaged in MDOL by affecting the amount of the final product exchange between the two populations. Nevertheless, in this scenario, the benefit from product privatization of the Embezzler strain cannot be completely eliminated by simply increasing substrate input.

We next included substrate toxicity into our model to test whether toxicity also affects community assembly (corollary 2). To this end, we performed simulations across three different toxic strength of the substrate as well as eight initial substrate concentration, and compared these results with previous results from the non-toxic scenario. Consistent with corollary 2, increasing substrate toxicity favors the 'Detoxifier' population (Figure 2A and B; Supplementary video 3). Our analyses further revealed that Detoxifier cells hold a lower intracellular concentration level of substrate (around 0.5 C-mmol/L less) than Embezzler cells across all the conditions (Supplementary Figure 4), due to its conversion reaction, thus possessing a growth advantage over the detoxifier cells. Intriguingly, when the initial substrate concentration and substrate toxicity sufficiently high, Detoxifier population are able to dominate the community (that is, its relative frequency exceeded 50% of the community; see Figure 2B),

suggesting that the benefit from product privatization of the Embezzler can be neutralized by higher substrate concentration and higher substrate toxicity.

To quantitively combine the effects of these two factors, we fit the simulation results by applying a simple polynomial function (named as PF1),

$$\boldsymbol{DF = 0.35 + 0.216\sqrt[3]{t} - \frac{2.5}{S}}$$

where $\boldsymbol{DF}$ represents the fraction of the 'Detoxifier' population; $\boldsymbol{S}$ is the substrate concentration; $\boldsymbol{t}$ is the toxic strength of the substrate; 0.35 is the maximum frequency of Detoxifier populations when substrate is non-toxic ($t = 0$). The function fits well with the simulation data (Supplementary Figure 5A; $R^2 = 0.960$), and suggests a simple rule about how substrate concentration and toxicity govern the assembly of community involving MDOL: the frequency of the 'Detoxifier' increases nonlinearly with the increase of the initial substrate concentration, but holds a maximum value determined by substrate toxicity. Specifically, when *t* exceeds approximately 0.335, the maximum frequency of the 'Detoxifier' population can exceed 0.5, i.e., the private benefit of the Embezzler is neutralized.

We then investigated whether MDOL affects the levels of intermixing of the populations in microbial communities. Therefore, we compared patterns developed in our basic model with those in a modified model considering that the two populations directly compete for a limited resource (See Supplementary Information S1 for the construction of this model). By analyzing the spatial assortment (See Methods and Supplementary Information S1 for the definition) of the cells in these patterns, we found that the presence of MDOL generally increases the intermixing level of the two strains

in the community in most of the conditions (Figure 2C). However, the effect was correlated with the substrate concentration and toxicity. In 'Competition' scenarios, higher the substrate concentration is associated with increased intermixing level. As shown in Figure 2C, the spatial assortment decreases from 0.68±0.06 (S = 5.0 C-mmol/L) to 0.32±0.13 (S = 40 C-mmol/L), due to the thickened active cell layer during the range expansion as reported previously[18]. In contrast, in MDOL scenarios, both increasing substrate concentration and increasing the toxicity of the substrate reduced the intermixing level of the two strains in the formed spatial pattern (Figure 2C; Supplementary 6), as both strains formed large clusters under these conditions (Figure 2A). In summary, our simulations clearly showed that when compound degradation pathway is executed through MDOL in a community, both increasing substrate input and increasing the toxicity of the substrate favor the Detoxifier population, as well as reducing the levels of intermixing of the interacting populations in the formed pattern.

Construction of a synthetic microbial community engaged in MDOL

We next tested our model prediction by engineering a synthetic community composed of two *P. stutzeri* strains, both of which degrade an organic compound, salicylate, via metabolic division of labor (Figure 3). We engineered both strains from an ancestral strain, *P. stutzeri* AN0011, which is capable of autonomously degrading salicylate (Supplementary Figure 7). An operon located in the chromosome of AN0011 contains a series of the genes encoding the enzymes responsible for the conversion of salicylate (Figure 3A), which was previously engineered to be regulated by an IPTG-inducible P_{tac} promoter (unpublished data; Figure 3B). To construct the 'Detoxifier' strain *P.*

stutzeri AN0010, we modified strain AN0011 by knocking out its *nahH* gene encoding catechol 2,3-dioxygenase, thus it was not capable of performing the second step. In addition, the *nahG* gene encoding salicylate 1-hydroxylase was deleted from AN0011 to generate the 'Embezzler' strain *P. stutzeri* AN0001 (Figure 3A and B). In addition, a strain lacking both *nahG* and *nahH* genes (Figure 3B) was constructed to serve as control strain that lacked the enzymes for both reaction steps, which we named 'Cheater'. Our analysis of enzymatic activity showed that Detoxifier only retained its ability to convert salicylate, while Embezzler was only able to metabolize the intermediate catechol (Supplementary Figure 7A). In liquid media, none of the Detoxifier, Embezzler, and Cheater strains grew autonomously using salicylate as the sole carbon source. However, Embezzler was capable of growing using catechol as the sole carbon source (Supplementary Figure 7B). When we co-cultured Detoxifier and Embezzler supplemented with a suitable range of concentration of salicylate, we found that the community grew at normal rates (Supplementary Figure 8A) and increasing the initial concentration of salicylate favored the 'Detoxifier' population in the final community, an observation that is in agreement with our model (Supplementary Figure 8B). As the intermediate catechol, cannot be directly used as the carbon source by both strains, the Embezzler strain possessed the preferential access to the final product, i.e., pyruvate and Acetyl-CoA (Figure 3A), which represented the direct carbon sources for the two strains in this community, consistent with our model assumption. In addition, salicylate was previously shown to be toxic for these *P. stutzeri* strains[31]. We quantitively measured its toxic strength (see Methods section measurement details). As

shown in Figure 3C, the value of its toxic strength ($\boldsymbol{t}$) was 0.62 L^{-1} C-mmol. Together, these results suggested that our synthetic community is suitable to experimentally test our hypotheses. For simplicity, we henceforth refer to our community as 'SMC-mdol'.

Substrate concentration and toxicity govern the assembly and spatial organization of the SMC-mdol

To experimentally test whether substrate concentration and toxicity affect the assembly and spatial organization of community engaged in MDOL, we cultured the SMC-mdol community on an agarose surface (Figure 4A, second row) to which salicylate was added at different concentrations. To perform the corresponding mathematical simulations, we included the experimental scenarios (for example, one-unit salicylate would be converted to two-unit final product, i.e., one pyruvate and one acetyl-CoA) to our original model (Figure 4A, first row; denoted as 'Model'; see Supplementary Information S1 sections for detail about the model modification). We analyzed the structures of the synthetic community in different conditions, which indicate that the relative frequency of the Detoxifier population increased with the improvement of initial substrate concentration. As shown in Figure 4B, the frequency of Detoxifier population varied from 11.2% ± 1.7% to 87.9% ± 6.4% as a function of substrate concentration, exhibiting the same trends as obtained from our simulations, indicating that substrate concentration governs the assembly of microbial community engaged in MDOL (Figure 4B). Importantly, when the substrate input reached high levels, the Detoxifier population dominated the community (i.e., its relative fraction over 50 %), suggesting that substrate toxicity considerably affect the assembly of the community.

Next, we generated a new fit function (named as PF2) based on our modified model related to the experimental scenarios (Supplementary Figure 5B; $R^2 = 0.986$) to make quantitive prediction about the assembly of the community. PF2 shows the same form as PF1, but values of the coefficients exhibited slightly differences, as follow

$$\boldsymbol{DF = 0.49 + 0.144\sqrt[3]{t} - \frac{1.25}{S}}$$

We then applied the measured value of toxic strength of salicylate (0.62) to this function to quantitively predict the final frequency of the Detoxifier population. As shown in Figure 4B (purple dashed line), the predictive power (Adjusted R^2) was 0.51. This result suggested that the assembly of our synthetic community follow the simple rule we proposed before, governed by substrate concentration and toxicity.

To examine the effects of substrate concentration and toxicity on spatial organization of the community, we calculated the spatial assortment of the patterns formed by our community and observation is similar as the model prediction, in which higher substrate concentration shaped a pattern with lower intermixing level of the two strains (Figure 4C). Nevertheless, the detail morphologies of the colony patterns showed some different characteristics compared with the simulated results. Firstly, at the edge of the developed colony, small 'sectors' were observed (Figure 4A, first row), which is usually explained by 'active layer effect' since limited resources are supplied and diffused from outside of the colony[18]. However, in our model, the only growth-limiting resource, P, is produced by Embezzler cells, thus is supplied from more inside place of the colony. Further to this simple assumption, resources in addition to the carbon source such as nitrogen or phosphorus, were also growth-limiting in the experimental culturing system,

and were supplied from outside of the colony. To overcome this difference, we introduced another limiting resource into the basic model. This resource is initially evenly supplied in the habitats and equally essential for the growth of both populations (Supplementary Figure 9A). This modification faithfully reproduced the 'sector' area in our further simulations (Figure 4A, denoted as 'Model-sectors'; Supplementary Figure 9B; Supplementary video 4). In addition, we generated an updated fit function (named as PF3) on the final frequency of the Detoxifier based on our new model (Supplementary Figure 5C; $R^2 = 0.984$), namely

$$\boldsymbol{DF = 0.49 + 0.157\sqrt[3]{t} - \frac{1.25}{S}}$$

PF3 only exhibited a slight shift of the coefficient compared with PF2 and predicted the assembly of the SMC-mdol with the predicting power (Adjusted R^2) of 0.52 (Figure 4B, blue dashed line), indicating that this modification negligibly affects our rule on the assembly of community engaged in MDOL.

Secondly, the Detoxifier cells within the colony grew and formed bubble-like structures, while the Embezzler cells located around these bubbles (Figure 4A; Supplementary Figure 10A). Image analysis of these bubble structure clearly showed that the Detoxifier cells gathered together, exhibiting a 'bowl'-like geometrical morphology (Supplementary Figure 10B). Our analysis of the fluorescence intensity of the two cell types showed that Embezzler cells were mostly distributed around the bubble formed by the Detoxifier (Supplementary Figure 10C), suggesting that the interaction between the two populations required their cells spatially proximal to each other. Intriguingly, we found that the size of the 'bubble' structures formed by the Detoxifier population

also changed with the increase of initial substrate concentration (Figure 4A, second row). We quantified this change by performing a segmentation imaging analysis of the 'bubble' area (Figure 5A), which indicated that with an increase in substrate concentration, while the number of the bubbles remained largely unchanged (Figure 5B), the average size of bubbles inside a colony significantly increased (Figure 5C), varying from 0.049 ± 0.010 mm^2 to 0.569 ± 0.067 mm^2. This suggests that Detoxifier cells tends to form larger cell clusters ('bubble' structures) with an increase in substrate concentration, resulting in lower intermixing levels of the two populations in the patterns (Figure 4C). Taken together, these results indicate that substrate concentration and toxicity govern the assembly and spatial organization of our synthetic community.

Deficiency of the type IV pili of the both strains resulted in a spatial pattern more similar as the simulated one

Although the assembly of the SMC-mdol community resulted in a considerable match with our model prediction, the detail morphologies of the colonies differed only slightly (that is, the 'bubble' structures) with the simulated ones. Therefore, we assumed that, beside interplay via MDOL, other factors contributed to the formation of 'bubble' structures. It has been reported that cell appendages, such as type IV pilus and flagellum, play important roles in the *Pseudomonas* biofilm formation[32-34]. To investigate if these cell structures were involved in the 'bubble' formation, we knocked out the related genes. To deactivate the type IV pili, we simultaneously knocked out *pilA* and *pilB* genes of both AN0010 and AN0001. We also deleted *flgL* and *flgK* genes of the two strains to disrupt their flagella. Therefore, in addition to the SMC-mdol community, by

co-culturing the pili deficient pair and flagella deficient pair, we constructed two additional synthetic communities named as 'SMC-mdol△*pilAB*' and 'SMC-mdol△*flgLK*'. Interestingly, while the SMC-mdol△*flgLK* community still developed into patterns with 'bubble' structures inside, the community SMC-mdol△*pilAB* self-organized to a colony that better resembled the colony developed in our mathematical simulations (Figure 6A). We also cultured our three synthetic communities supplementing one of the final products, pyruvate, as the sole limited resource to simulate the 'competition' scenario, resulted in the segregated patterns as our model predictions (Figure 6A). Our analysis of spatial assortment revealed that MDOL between the two cell types generally increases their levels of intermixing, compared with those 'competition' scenarios (Figure 6B, unpaired, two-tailed, Student's t-test between the two scenarios of the three communities, $p<0.01$). In addition, deficiency of the type IV pili further drives cells of the two strains to translocate into closer proximity? (Figure 6B, $p<0.01$). Moreover, compared with the pattern formed by the SMC-mdol community and the SMC-mdol△*flgLK* community, colonies developed by the community SMC-mdol△*pilAB* produced more biomass, (Figure 6C, $p<0.01$), suggesting that spatial proximity to each other facilitates the interaction between the two cell types, leading to better community-level productivity. In summary, these results strongly suggested that type IV pili are essential for the formation of the 'bubble' structures.

To further test our proposed rule, we cultured the SMC-mdol△*pilAB* community on agarose surface supplemented with different initial substrate concentration (Figure 4A,

fourth row). We found the frequency of Detoxifier population increased from 29.4% ± 2.8% to 79.2% ± 2.6%, which better agreed with the results obtained from the simulations (Figure 4B). Notably, at high substrate levels, the Detoxifier population also dominated the community (i.e., its relative fraction over 50 %). This result suggests that substrate toxicity affected the assembly of the SMC-mdol△*pilAB* community in a similar manner observed in the SMC-mdol community. In addition, both PF2 (Adjusted R^2 equals 0.76) and PF3 (Adjusted R^2 equals 0.78) predict the assembly of the SMC-mdol△*pilAB* community better than that of the SMC-mdol community. These results suggest that after excluding the effect of type IV pili, the assembly of synthetic community involving MDOL can be better predicted from the proposed rule. To quantify the spatial patterns developed by the SMC-mdol△*pilAB* community, we calculated the values of their spatial assortment, confirming the trend predicted by the model simulations (Figure 4C and D). In summary, culture experiments with the SMC-mdol△*pilAB* community again indicates that substrate concentration and toxicity govern the assembly and spatial organization of microbial community involving MDOL.

Discussion

Here we show that substrate concentration and its toxicity drive the assembly of the microbial communities engaged in metabolic division of labor (MDOL), in which the population performing the first step is favored by both higher substrate concentration and its toxicity. We also found that the levels of intermixing between the interacting populations decreased with the increase of substrate concentration and toxicity, resulted in different spatial patterns.

Previous studies based on meta-omics approach revealed that MDOL were present in many microbial communities specialized in degrading organic compounds[6,35]. Inspired by these natural MDOL systems, numerous studies have recently explored strategies to divide metabolic roles across different populations in a consortium toward removal of organic pollutants[36-41]. While most of these studies only focused on the efficiency in pollutant degradation of these communities, a few of studies measured their community structures. For instance, one earlier study developed a dual-species community for biodegradation of the insecticide parathion[42]. In this consortium, an *Escherichia coli* strain SD2 was responsible for hydrolyzing parathion (Detoxifier), yielding two intermediates including p-nitrophenol, while another *Pseudomonas putida* strain KT2440 was responsible for metabolizing p-nitrophenol (Embezzler). That study found that the strain KT2440 that largely dominated the biofilm formed by this community, which is squarely in agreement with our basic prediction that the Embezzler strain is generally favored due to the 'private benefit'. Another study investigated the interactions among five bacterial species in a cellulose-degrading community, which

409 also found that the strains responsible for the last step of the cellulose degradation
410 constituted more than 60 percent of the total population[43]. Moreover, one recent study
411 reported that a bacterial consortium composed of *Leucobacter* sp. GP and
412 *Achromobacter denitrificans* PR1 efficiently degrades an antibiotic, sulfamethoxazole,
413 in which the strain GP is responsible for the initial metabolism of the sulfamethoxazole
414 (Detoxifier), and the strain PR1 carries out the subsequent conversion (Embezzler)[44].
415 This study measured the structures of the community across a gradient of initial
416 substrate concentrations, and found that the frequency of the GP is positively correlated
417 with the initial sulfamethoxazole concentration. This observation largely agrees idea
418 derived from our model and experiments that increasing concentration of the substrate
419 favors the Detoxifier population. Therefore, the proposed rule in our study may be
420 expanded to forecast the assembly of other communities engaged in MDOL.
421 Based on our individual-based modelling, we showed that substrate toxicity is vital to
422 govern the assembly of communities engaged in MDOL. However, due to the difficulty
423 of manipulating the toxicity of the substrate (salicylate) *in vitro*, we did not
424 experimentally compare the impacts of different toxic strength on the community
425 assembly. However, our model predicts that simply increasing the initial substrate
426 concentration is unlikely to shape a community dominated by the Detoxifier population,
427 while the presence of substrate toxicity renders the dominance of the 'Detoxifier'
428 population in the community. Therefore, the truth that Detoxifier population was able
429 to dominate the synthetic community within higher substrate input, and the measured
430 biotoxicity of salicylate, strongly suggested that substrate toxicity should be included

in the assembly of the synthetic microbial community. Consistent with this idea, the prediction function (PF2 and PF3) involved in salicylate toxic strength fits the experiment results very well. To further examined this idea, we need to design a better synthetic community in which the toxicity of the substrate can be modulated. For example, several studies applied defined co-culture of multiple bacterial species to degrades antibiotics[44-46]. In these systems, antibiotics are toxic to all strains involved, but their toxicity may be modulated by genetically modifying the expression of the genes encoding the related antibiotic resistance. Performing pattern formation assays using these well-defined systems should assist in more thoroughly investigating the effects of substrate toxicity on the assembly of community.

In the colonies developed by SMC-mdol, we observed 'bubble'-like structures formed by the 'Detoxifier' cells, which has not been reported before. We found that the formation of these structures is highly correlated with the function of type IV pili. One important cell behavior mediated by type IV pili is bacterial twitching motility[47,48]. Indeed, we failed to observe twitching motility in mutants lacking *pilA* and *pilB* genes (Supplementary Figure 11). On the basis of this finding, we hypothesize that the observed 'bubble'-like structures were derived from active surface movement the *Pseudomonas* strains. Due to the heterogenous mass distribution of substrate or intermediates in environments that are spatially structured, the self-gathering behavior of our Detoxifier strain may be related to the chemotactic motility mediated by twitching motility[48,49]. Nevertheless, since type IV pili were also reported to be involved in other aspects of bacterial biofilm formation, such as surface sensing[50] and

surface attachment[51,52], which may also contribute to the ‘bubble’ formation observed in our experiments. How these types of single-cell behavior shape the macroscopic colony pattern requires more detailed investigation at the single-cell level.

The ability to predict how the communities assembled by a given set of strains exhibiting modularized functions is fundamental to engineer stable and high-efficient microbial systems for bioproduction or biodegradation. Our results demonstrate that, for a given community engaged in MDOL, its assembly can be quantitatively predicted from the traits of its substrate, suggesting that it is feasible to control and manage microbial communities through manipulation of environmental factors.

Methods

Individual-based modeling

The model was based on *gro* platform (https: https://github.com/liaupm/GRO-LIA), a simulator designed by Gutiérrez and colleagues aiming to describe multicellular bacterial behavior[53]. custom codes were written in *gro* language to describe interaction between two populations who implemented substrate degradation via MDOL. Supplementary Figure 2 provides an overview of the mathematical logic of the model. Variables and Parameters are summarized in Supplementary Table 1 and Supplementary Table 2, respectively. Details of the model framework and simulation workflow are described in Supplementary Information S1. The source *gro* codes of all the simulations used in this study, as well as the Mathematica (version 12.0) codes used for data analyses are available at Github: https://github.com/RoyWang1991/MDOLcode/tree/master/MDOL-spatial.

Construction of the *P. stutzeri* strains

All *P. stutzeri* strains were engineered from a naphthalene-degrading bacterial strain *P. stutzeri* AN10[54]. *P. stutzeri* AN0011 is a derived strain that can degrade salicylate autonomously, and all the genes encoding the corresponding enzymes were located in an operon induced by IPTG (unpublish data). To generate *P. stutzeri* AN0010 and *P. stutzeri* AN0001, *nahG* or *nahH* gene of *P. stutzeri* AN0011 was knocked out, respectively. Strain *P. stutzeri* AN0000 was generated from knocking out *nahH* gene of *P. stutzeri* AN0001. To generate the pilus mutants or flagellum mutants, *pilA* and *pilB* genes, or *flgL* and *flgK* genes, were simultaneously removed from the host strains,

484 respectively. The genetic manipulation was implemented by allele exchange using the
485 suicide plasmid pK18mobsacB[55,56]. The constructed strains were validated by PCR and
486 DNA sequencing. In addition, enzymic activity assays were performed to verify the
487 construction of *P. stutzeri* AN0011, *P. stutzeri* AN0010, *P. stutzeri* AN0001, as well as
488 *P. stutzeri* AN0000, following the methods reported before (ref for salicylate 1-
489 hydroxylase and ref for catechol 2,3-dioxygenase). Furthermore, agar-based 'stab'
490 assays were performed to validate the pilus mutants (Supplementary Figure 11), while
491 'swimming' assays were performed to validate flagellum mutants (Supplementary
492 Figure 12), both following the standard protocol[57]. To label the strains with
493 fluorescence, *mCherry* or *eGFP* was cloned into a constitutive vector, pMMPc-Gm[58],
494 and delivered to the host cells via triparental filter mating[56].

495 **Liquid cultivation of the *P. stutzeri* strains**

496 To prepare the inoculum, *P. stutzeri* strains were first grown at 30˚C RB liquid medium
497 (Yeast extract 10 g/L, beef extract 6 g/L, peptone 10 g/L, ammonium sulfate 5 g/L) by
498 shaking at 220 rpm, supplemented with 50 μg/mL gentamicin. The cells were then
499 washed by the minimum medium[59] for twice to make an inoculum. For co-culture
500 experiments, inocula of two strains the were concentrated to an Optical density (OD,
501 measured at 600 nm) of 5.0, and mixed at a 1:1 ratio, and then inoculated to a 25-mL
502 flask containing 5 mL new fresh minimum medium (starting OD: 0.05), supplemented
503 with 2 mM IPTG, 50 μg/mL gentamicin, as well as salicylate as the sole carbon source.
504 For mono-culture experiments, conditions were identical except the fact that the
505 inoculum of one single strain was inoculated. Culture liquid (100 μL) was taken from

system to measure OD to estimate the total biomass, as well as measure fluorescence intensity to estimate the growth of each population. The relative fraction was calculated by a method previously described[60]. Briefly, cultures of each populations were grown to mid-log phase at 30˚C (OD: ~0.3), diluted two-fold for eleven times, and the dilutions measured for their OD and fluorescence. Correlations between OD and fluorescence were then determined using the basic method defined in the LinerModelFit function of Mathematica software. Eventually, fluorescence values were transformed to the OD-estimated biomass to assess the growth of each population, and relative fraction was then calculated. These measurements, as well as the related measurements described below, were performed using a microplate reader (Molecular Devices, Sunnyvale, America).

Measurement of salicylate toxicity

The exact toxic strength of salicylate was measured using a homologous strain *P. stutzeri* AN0000, named as 'Cheater' (Figure 3B), which lacks both *nahG* and *nahH* genes, thus cannot performed both steps. This strain was cultured in minimum medium by supplying sufficient amount of final product pyruvate (0.34 mol/L, which means adding more pyruvate will no longer increase the bacterial growth rate) and varied amount of toxic salicylate. Growth curves were then estimated for every salicylate concentration, and the data fitted to calculate the specific growth rate $\boldsymbol{g_s}$ by a Boltzmann function using the Nonlinearmodelfit function of the Wolfram Mathematica (version 12.4). Subsequently, the following model was applied to fit the growth rate with the salicylate concentration:

$$g_s = g_{max} \cdot \left(\frac{1}{1+t \cdot S}\right) - d$$

, where g_{max} is the growth rate in absence of salicylate; d is the one-dimensional death rate. The resulting fitted Adjust correlation coefficient (R^2) was 0.965 and the quantified toxic strength of salicylate was 0.62 (Figure 3C).

Colony pattern formation assays

Inoculation and cultivation. Minimum medium (1.5% agarose, Takara, Dalian, China), supplemented with 2 mM IPTG, 50 μg/mL gentamicin, and supplying salicylate or pyruvate as sole carbon source, was used in these studies. To prepare the culture plate, five milliliters of this medium was poured in a Petri dish (60 mm in diameter) and left on the bench overnight before inoculation. Preparation of the inocula is performed by the same way as liquid cultivation section. Inocula of two strains were then concentrated to an OD of 1.0, and mixed at a 1:1 ratio. For each colony, 1 μl of the inoculum was spotted on the prepared plate, after which it was allowed to dry for 10 min. After the inoculum dried on the plate, the plates were incubated at 30 ˚C for 120 h.

Microscopy imaging. Colony patterns were imaged under 5× objective using a Leica DM6000B fluorescence microscope (Leica Corporation, Wetzlar, Germany) equipped with a LED fluorescence illuminator (Leica Corporation). Images were sequentially recorded with a DFC360 FX camera (Leica Corporation) using a GFP filter cube for eGFP (exciter: 475/40; emitter: 525/50: beamsplitter: 495) and a TX2 filter cube for mCherry (exciter: 560/40; emitter: 645/75: beamsplitter: 595). Tile scan function of Leica LAS X acquisition software (Leica Microsystems) were applied to assemble the

full view of a colony from multiple fields, and composite images were also created by this software.

Confocal imaging. To investigate the 3D structure of the 'bubble'-like structure, typical bubble areas were imaged under 10× objective using an Andor Revolution XD laser confocal fluorescence microscope (Andor, Oxford, UK) associated with ANDOR Zyla sCOMS camera. Individual color channels were acquired using the FLIC and TxRed filters in addition to a bright-field channel. The images were assembled and virtualized in Image J software (version 1.53c). In addition, 'Surface Plot' function of Image J software was applied to analyze the relative intensity of fluorescence across the bubble areas.

Imaging analysis. Wolfram Mathematica (version 12.4) was used to process and analyze images. For the quantification of spatial assortment of each colony, the assembled eGFP and mCherry images were separately exported as grayscale tiff files, and then resized into images with 1000 pixels wide (using ImageResize function) to reduce computation time. Then ColorQuantize function was used to give an approximation to the image by quantizing it to distinct colors, subsequently transform the images into binarized data using ImageData function. Values of spatial assortment were calculated followed the protocol previous reported[61,62], using these binarized matrix data as the input. Assortment is defined as the Embezzler segregation within their local neighborhood measured relative to its global frequencies. The Embezzler segregation was calculated by

$$seg(E_i) = \frac{1}{n_e}\sum_{j=1}^{n_e} g(E_i, E_j)$$

where n_e is the number of cells falling within the distance of 50 pixels; $g(E_i, E_j) = 0$ if E_i and E_j belong to different populations, or, $g(E_i, E_j) = 1$ if E_i and E_j belong to the same population. The spatial assortment was then calculated by

$$Assor = \frac{\frac{1}{N_e}\sum_{j=1}^{N_e} seg(E_i) - \mathrm{F}_e}{1 - \mathrm{F}_e}$$

where N_e is the total number of Embezzler cells in the colony; F_e is the frequency of Embezzler cells in the colony. This value is bounded between -1 and 1, while assortment values of zero reflect a well-mixed colony. For the quantification of the bubble structure of each colony, color channel related to the 'Detoxifier' was used. We first cropped the images to focus on the inside area containing 'bubbles'. Then the 'bubbles' were segmented by the watershed algorithm using the WatershedComponents function of the Wolfram Mathematica, followed by obtained the statistic data of the number and size of these structures by using ComponentMeasurements function. The area size in pixels were finally transformed to be the real size (in mm^2) by multiply the scale bar, and virtualized by Colorize function. All these calculations were performed in custom Wolfram Mathematica scripts. The source codes used are available on Github: https://github.com/RoyWang1991/MDOLcode/tree/master/MDOL-spatial.

Measurements of biomass and relative fraction. To estimate the biomass and community composition of a colony, spot was collected by an inoculation loop from the plate after 120-h's culture, and bacterial cells were resuspended in 100 μL minimum medium and vortexed for 10 min to destruct the biofilms. After that, the OD was

measured to estimate the total biomass, and fluorescence intensities of eGFP and mCherry were measured to estimate the growth of each population. Calculation of the relative fraction followed the same method described in the Liquid cultivation section.

Statistical analyses

Unless indicated otherwise, the number of replicates is eight for each simulation and six for each experiment. For comparative statistics, unpaired, two-tailed, Student's t-test was performed in Wolfram Mathematica (version 12.4). To fit the data to the proposed function, Nonlinearmodelfit function of the Wolfram Mathematica (version 12.4) were applied.

Competing Interests

The authors declare that they have no conflict of interest.

Acknowledgments

We wish to thank Dr. Min Lin (Chinese Academy of Agricultural Sciences, Beijing, P.R. China) for providing plasmid pK18mobsacB and pRK2013, used for genetic engineering in this work. We also thank Professor Ping Xu (Shanghai Jiao Tong University, Shanghai, P.R. China) for supplying plasmid pMMPc-Gm, used for fluorescence labeling in this study. We are grateful to Professor Martin Ackermann (ETH Zurich, Zurich, Switzerland), Dr. David Johnson (Eawag, Dübendorf, Switzerland) and Yinyin Ma (Eawag, Dübendorf, Switzerland) for constructive inputs on the design of this study. We also appreciate Professor Martín Gutiérrez (Universidad Politécnica de Madrid, Madrid, Spain) for his kindly guidance for the set-up of the *gro* platform for the individual-based simulations. This work was supported by National

Key R&D Program of China (2018YFA0902100 and 2018YFA0902103), and National Natural Science Foundation of China (91951204, 31761133006, 31770120, and 31770118).

References

1 Kreft, J. U., Griffin, B. M. & Gonzalez-Cabaleiro, R. Evolutionary causes and consequences of metabolic division of labour: why anaerobes do and aerobes don't. *Curr Opin Biotechnol* **62**, 80-87, doi:10.1016/j.copbio.2019.08.008 (2020).

2 Tsoi, R. *et al.* Metabolic division of labor in microbial systems. *Proc Natl Acad Sci U S A* **115**, 2526-2531, doi:10.1073/pnas.1716888115 (2018).

3 Harvey, E., Heys, J. & Gedeon, T. Quantifying the effects of the division of labor in metabolic pathways. *J Theor Biol* **360**, 222-242, doi:10.1016/j.jtbi.2014.07.011 (2014).

4 Thommes, M., Wang, T., Zhao, Q., Paschalidis, I. C. & Segre, D. Designing Metabolic Division of Labor in Microbial Communities. *mSystems* **4**, doi:10.1128/mSystems.00263-18 (2019).

5 Seelke, R. The Prokaryotes: a handbook on the biology of bacteria. *Choice: Current Reviews for Academic Libraries* **45**, 68-68 (2007).

6 Dombrowski, N. *et al.* Reconstructing metabolic pathways of hydrocarbon-degrading bacteria from the Deepwater Horizon oil spill. *Nat Microbiol* **1**, 16057, doi:10.1038/nmicrobiol.2016.57 (2016).

7 West, S. A. & Cooper, G. A. Division of labour in microorganisms: an evolutionary perspective. *Nat Rev Microbiol* **14**, 716-723, doi:10.1038/nrmicro.2016.111 (2016).

8 van Gestel, J., Vlamakis, H. & Kolter, R. Division of Labor in Biofilms: the Ecology of Cell Differentiation. *Microbiol Spectr* **3**, MB-0002-2014, doi:10.1128/microbiolspec.MB-0002-2014 (2015).

9 Lilja, E. E. & Johnson, D. R. Segregating metabolic processes into different microbial cells accelerates the consumption of inhibitory substrates. *Isme Journal* **10**, 1568-1578, doi:10.1038/ismej.2015.243 (2016).

10 Schink, B. & Pfennig, N. Fermentation of Trihydroxybenzenes by Pelobacter-Acidigallici Gen-Nov Sp-Nov a New Strictly Anaerobic, Non-Sporeforming Bacterium. *Arch Microbiol* **133**, 195-201, doi:Doi 10.1007/Bf00415000 (1982).

11 Wang, C. Y., Huang, Y., Zhang, Z. T., Hao, H. & Wang, H. Absence of the nahG-like gene caused the syntrophic interaction between Marinobacter and other microbes in PAH-degrading process. *J Hazard Mater* **384**, doi:10.1016/j.jhazmat.2019.121387 (2020).

12 Billet, L., Devers, M., Rouard, N., Martin-Laurent, F. & Spor, A. Labour sharing promotes coexistence in atrazine degrading bacterial communities. *Sci Rep* **9**, 18363, doi:10.1038/s41598-019-54978-2 (2019).

13 Koudryashova, Y., Chizhova, T., Tishchenko, P. & Hayakawa, K. Seasonal Variability of Polycyclic Aromatic Hydrocarbons (PAHs) in a Coastal Marine Area in the Northwestern Region of the Sea of Japan/East Sea (Possiet Bay). *Ocean Sci J* **54**, 635-655, doi:10.1007/s12601-019-0031-9 (2019).

14 Jiang, Y., Hu, X., Yves, U. J., Zhan, H. & Wu, Y. Status, source and health risk assessment of

polycyclic aromatic hydrocarbons in street dust of an industrial city, NW China. *Ecotoxicol Environ Saf* **106**, 11-18, doi:10.1016/j.ecoenv.2014.04.031 (2014).

15 Ozaki, N., Takamura, Y., Kojima, K. & Kindaichi, T. Loading and removal of PAHs in a wastewater treatment plant in a separated sewer system. *Water Res* **80**, 337-345, doi:10.1016/j.watres.2015.05.002 (2015).

16 Hall-Stoodley, L., Costerton, J. W. & Stoodley, P. Bacterial biofilms: from the natural environment to infectious diseases. *Nat Rev Microbiol* **2**, 95-108, doi:10.1038/nrmicro821 (2004).

17 Nadell, C. D., Drescher, K. & Foster, K. R. Spatial structure, cooperation and competition in biofilms. *Nat Rev Microbiol* **14**, 589-600, doi:10.1038/nrmicro.2016.84 (2016).

18 Nadell, C. D., Foster, K. R. & Xavier, J. B. Emergence of Spatial Structure in Cell Groups and the Evolution of Cooperation. *Plos Computational Biology* **6**, doi:10.1371/journal.pcbi.1000716 (2010).

19 Frost, I. *et al.* Cooperation, competition and antibiotic resistance in bacterial colonies. *Isme Journal* **12**, 1582-1593, doi:10.1038/s41396-018-0090-4 (2018).

20 Momeni, B., Waite, A. J. & Shou, W. Spatial self-organization favors heterotypic cooperation over cheating. *Elife* **2**, e00960, doi:10.7554/eLife.00960 (2013).

21 Knittel, K. & Boetius, A. Anaerobic oxidation of methane: progress with an unknown process. *Annu Rev Microbiol* **63**, 311-334, doi:10.1146/annurev.micro.61.080706.093130 (2009).

22 Boetius, A. *et al.* A marine microbial consortium apparently mediating anaerobic oxidation of methane. *Nature* **407**, 623-626, doi:10.1038/35036572 (2000).

23 Raghoebarsing, A. A. *et al.* A microbial consortium couples anaerobic methane oxidation to denitrification. *Nature* **440**, 918-921, doi:10.1038/nature04617 (2006).

24 Ettwig, K. F. *et al.* Archaea catalyze iron-dependent anaerobic oxidation of methane. *Proc Natl Acad Sci U S A* **113**, 12792-12796, doi:10.1073/pnas.1609534113 (2016).

25 Knittel, K., Losekann, T., Boetius, A., Kort, R. & Amann, R. Diversity and distribution of methanotrophic archaea at cold seeps. *Appl Environ Microb* **71**, 467-479, doi:10.1128/Aem.71.1.467-479.2005 (2005).

26 Nauhaus, K., Albrecht, M., Elvert, M., Boetius, A. & Widdel, F. In vitro cell growth of marine archaeal-bacterial consortia during anaerobic oxidation of methane with sulfate. *Environ Microbiol* **9**, 187-196, doi:10.1111/j.1462-2920.2006.01127.x (2007).

27 Losekann, T. *et al.* Diversity and abundance of aerobic and anaerobic methane oxidizers at the Haakon Mosby mud volcano, Barents Sea. *Appl Environ Microb* **73**, 3348-3362, doi:10.1128/Aem.00016-07 (2007).

28 Niemann, H. *et al.* Novel microbial communities of the Haakon Mosby mud volcano and their role as a methane sink. *Nature* **443**, 854-858, doi:10.1038/nature05227 (2006).

29 Tecon, R. & Or, D. Cooperation in carbon source degradation shapes spatial self-organization of microbial consortia on hydrated surfaces. *Sci Rep-Uk* **7**, doi:10.1038/srep43726 (2017).

30 Quintas, C., Leyva, J. S., Sotoca, R., Loureiro-Dias, M. C. & Peinado, J. M. A model of the specific growth rate inhibition by weak acids in yeasts based on energy requirements. *Int J Food Microbiol* **100**, 125-130, doi:10.1016/j.ijfoodmicro.2004.10.009 (2005).

31 Lanfranconi, M. P. *et al.* Physiological role of NahW, the additional salicylate hydroxylase found in *Pseudomonas stutzeri* AN10. *Fems Microbiol Lett* **300**, 265-272, doi:10.1111/j.1574-6968.2009.01787.x (2009).

32 Klausen, M. *et al.* Biofilm formation by *Pseudomonas aeruginosa* wild type, flagella and type IV pili mutants. *Mol Microbiol* **48**, 1511-1524, doi:10.1046/j.1365-2958.2003.03525.x (2003).

33 Barken, K. B. *et al.* Roles of type IV pili, flagellum-mediated motility and extracellular DNA in the formation of mature multicellular structures in *Pseudomonas aeruginosa* biofilms. *Environ Microbiol* **10**, 2331-2343, doi:10.1111/j.1462-2920.2008.01658.x (2008).

34 O'Toole, G. A. & Kolter, R. Flagellar and twitching motility are necessary for Pseudomonas aeruginosa biofilm development. *Mol Microbiol* **30**, 295-304, doi:10.1046/j.1365-2958.1998.01062.x (1998).

35 Yu, K. *et al.* An integrated meta-omics approach reveals substrates involved in synergistic interactions in a bisphenol A (BPA)-degrading microbial community. *Microbiome* **7**, 16, doi:10.1186/s40168-019-0634-5 (2019).

36 Li, Z. *et al.* Anaerobic mineralization of 2,4,6-tribromophenol to CO2 by a synthetic microbial community comprising Clostridium, Dehalobacter, and Desulfatiglans. *Bioresour Technol* **176**, 225-232, doi:10.1016/j.biortech.2014.10.097 (2015).

37 Che, S. & Men, Y. Synthetic microbial consortia for biosynthesis and biodegradation: promises and challenges. *J Ind Microbiol Biotechnol* **46**, 1343-1358, doi:10.1007/s10295-019-02211-4 (2019).

38 Hudcova, T., Halecky, M., Kozliak, E., Stiborova, M. & Paca, J. Aerobic degradation of 2,4-dinitrotoluene by individual bacterial strains and defined mixed population in submerged cultures. *J Hazard Mater* **192**, 605-613, doi:10.1016/j.jhazmat.2011.05.061 (2011).

39 Yang, C. *et al.* Atrazine degradation by a simple consortium of Klebsiella sp. A1 and Comamonas sp. A2 in nitrogen enriched medium. *Biodegradation* **21**, 97-105, doi:10.1007/s10532-009-9284-9 (2010).

40 Roell, G. W. *et al.* Engineering microbial consortia by division of labor. *Microb Cell Fact* **18**, 35, doi:10.1186/s12934-019-1083-3 (2019).

41 Jia, X. Q., He, Y., Jiang, D. W., Liu, C. & Lu, W. Y. Construction and analysis of an engineered Escherichia coli-Pseudomonas aeruginosa co-culture consortium for phenanthrene bioremoval. *Biochem Eng J* **148**, 214-223, doi:10.1016/j.bej.2019.05.010 (2019).

42 Gilbert, E. S., Walker, A. W. & Keasling, J. D. A constructed microbial consortium for biodegradation of the organophosphorus insecticide parathion. *Appl Microbiol Biot* **61**, 77-81, doi:10.1007/s00253-002-1203-5 (2003).

43 Kato, S., Haruta, S., Cui, Z. J., Ishii, M. & Igarashi, Y. Stable coexistence of five bacterial strains as a cellulose-degrading community. *Appl Environ Microb* **71**, 7099-7106, doi:10.1128/Aem.71.11.7099-7106.2005 (2005).

44 Reis, A. C. *et al.* Biodegradation of sulfamethoxazole by a bacterial consortium of *Achromobacter denitrificans* PR1 and *Leucobacter* sp GP. *Appl Microbiol Biot* **102**, 10299-10314, doi:10.1007/s00253-018-9411-9 (2018).

45 Liu, C. X., Xu, Q. M., Yu, S. C., Cheng, J. S. & Yuan, Y. J. Bio-removal of tetracycline antibiotics under the consortium with probiotics *Bacillus clausii* T and *Bacillus amyloliquefaciens* producing biosurfactants. *Sci Total Environ* **710**, doi:10.1016/j.scitotenv.2019.136329 (2020).

46 Kong, X. X. *et al.* The biodegradation of cefuroxime, cefotaxime and cefpirome by the synthetic consortium with probiotic *Bacillus clausii* and investigation of their potential biodegradation pathways. *Sci Total Environ* **651**, 271-280, doi:10.1016/j.scitotenv.2018.09.187 (2019).

47 Barken, K. B. *et al.* Roles of type IV pili, flagellum-mediated motility and extracellular DNA in the formation of mature multicellular structures in *Pseudomonas aeruginosa* biofilms. *Environmental Microbiology* **10**, 2331-2343, doi:10.1111/j.1462-2920.2008.01658.x (2008).

48 Oliveira, N. M., Foster, K. R. & Durham, W. M. Single-cell twitching chemotaxis in developing biofilms. *Proc Natl Acad Sci U S A* **113**, 6532-6537, doi:10.1073/pnas.1600760113 (2016).

49 Miller, R. M. *et al. Pseudomonas aeruginosa* twitching motility-mediated chemotaxis towards phospholipids and fatty acids: Specificity and metabolic requirements. *J Bacteriol* **190**, 4038-4049, doi:10.1128/Jb.00129-08 (2008).

50 Chang, C. Y. Surface Sensing for Biofilm Formation in *Pseudomonas aeruginosa*. *Frontiers in Microbiology* **8**, doi:10.3389/fmicb.2017.02671 (2018).

51 Beaussart, A. *et al.* Nanoscale Adhesion Forces of *Pseudomonas aeruginosa* Type IV Pili. *Acs Nano* **8**, 10723-10733, doi:10.1021/nn5044383 (2014).

52 Touhami, A., Jericho, M. H., Boyd, J. M. & Beveridge, T. J. Nanoscale characterization and determination of adhesion forces of *Pseudomonas aeruginosa* Pili by using atomic force microscopy. *J Bacteriol* **188**, 370-377, doi:10.1128/Jb.188.2.370-377.2006 (2006).

53 Gutierrez, M. *et al.* A New Improved and Extended Version of the Multicell Bacterial Simulator gro. *ACS Synth Biol* **6**, 1496-1508, doi:10.1021/acssynbio.7b00003 (2017).

54 Brunet-Galmes, I. *et al.* Complete Genome Sequence of the Naphthalene-Degrading Bacterium *Pseudomonas stutzeri* AN10 (CCUG 29243). *J Bacteriol* **194**, 6642-6643, doi:10.1128/Jb.01753-12 (2012).

55 Schafer, A. *et al.* Small mobilizable multi-purpose cloning vectors derived from the *Escherichia coli* plasmids pK18 and pK19: selection of defined deletions in the chromosome of *Corynebacterium glutamicum*. *Gene* **145**, 69-73, doi:10.1016/0378-1119(94)90324-7 (1994).

56 Gao, C. *et al.* NAD-Independent L-Lactate Dehydrogenase Required for L-Lactate Utilization in *Pseudomonas stutzeri* A1501. *J Bacteriol* **197**, 2239-2247, doi:10.1128/JB.00017-15 (2015).

57 Filloux, A. & Ramos, J. L. Preface. *Pseudomonas* methods and protocols. *Methods Mol Biol* **1149**, v, doi:10.1007/978-1-4939-0473-0 (2014).

58 Xu, Y., Tao, F., Ma, C. & Xu, P. New constitutive vectors: useful genetic engineering tools for biocatalysis. *Appl Environ Microbiol* **79**, 2836-2840, doi:10.1128/AEM.03746-12 (2013).

59 Liang, J. L. *et al.* Regulation of alkane degradation pathway by a TetR family repressor via an autoregulation positive feedback mechanism in a Gram-positive *Dietzia* bacterium. *Mol Microbiol* **99**, 338-359, doi:10.1111/mmi.13232 (2016).

60 Adamowicz, E. M., Flynn, J., Hunter, R. C. & Harcombe, W. R. Cross-feeding modulates antibiotic tolerance in bacterial communities. *Isme Journal* **12**, 2723-2735, doi:10.1038/s41396-018-0212-z (2018).

61 Estrela, S. & Brown, S. P. Metabolic and demographic feedbacks shape the emergent spatial structure and function of microbial communities. *PLoS Comput Biol* **9**, e1003398, doi:10.1371/journal.pcbi.1003398 (2013).

62 Yanni, D., Marquez-Zacarias, P., Yunker, P. J. & Ratcliff, W. C. Drivers of Spatial Structure in Social Microbial Communities. *Curr Biol* **29**, R545-R550, doi:10.1016/j.cub.2019.03.068 (2019).

Figure Legends

Figure 1 Hypotheses for how substrate concentration and toxicity govern the assembly of community involving MDOL. In a community degrading an organic compound through metabolic division of labor (MDOL), final product was assumed to be the sole resource and was synthesized by the strain performing the last step. Therefore, this strain will obtain more nutrients (denoted as bigger 'smiling face'), while the other strain has to collect product released from this population (denoted as smaller 'smiling face'). Thus, the last population was named 'Embezzler'. However, increasing the concentration of the substrate (vertical axis) improves the flux of the pathway, leading to higher final product leakiness, favoring the growth of the first population. Moreover, introducing substrate biotoxicity (horizontal axis) also favors the first population, because it performs conversion of this toxic substrate (denoted as smaller sad face), resulted in lower intracellular substrate concentration than the Embezzler cells (denoted as bigger sad face). Thus, the first population was named as 'Detoxifier'.

Figure 2 Individual-based modelling suggests that substrate concentration and toxicity govern the assembly and spatial organization of community involving MDOL. (A) Representative colony patterns from the simulations in 'MDOL' scenarios across eight kinds of initial substrate concentrations and four different toxic strength, as well as the patterns developed when two populations simply compete for P ('Competition' scenarios). (B) Analysis of community composition of these colonies. Plot shows the relationship between substrate concentration and toxicity with the relative fraction of Detoxifier cells. (C) Analysis of spatial assortment (intermixing level) of these colonies. Here, an assortment value of 0 means cells of the two populations is randomly distributed (i.e., a well-mixed pattern), while a value of 1 means the distribution of the two populations is totally segregated. Plot shows the relationship between substrate concentration and toxicity with the spatial assortment of the colonies. As described in Methods

806 section, the closer that the assortment value to zero means the corresponding pattern is more mixed. All
807 the data were collected when the number of cells in the colony just reached 8100. Eight replicated
808 simulations were performed for each condition.

809 **Figure 3** Design of the SMC-mdol. (A) Pathway of salicylate degradation in 'Superman' strain *P. stutzeri*
810 AN0011, as well as partial pathways carried out by Detoxifier strain AN0010 and Embezzler strain
811 AN0001. Skull marks that salicylate is toxic. (B) Diagram of operons responsible for the salicylate
812 degradation, located in the chromosomes of AN0011, AN0010, AN0001 as well as a homologous mutant
813 AN0000. (C) Determination of the toxic strength of the substrate salicylate. We measured the growth rate
814 of AN0000 using pyruvate, one of the end products, as the carbon source, and supplying different
815 concentration of salicylate. The growth rates ($\boldsymbol{g_s}$) were fitted with the corresponding salicylate
816 concentration ($\boldsymbol{S}$), using a formula involving maximum growth rate ($\boldsymbol{g_{max}}$) and one-dimensional death
817 rate ($\boldsymbol{d}$), showing a hyperbolic toxic effect (See Methods section for detailed description).

818 **Figure 4** Substrate concentration and toxicity govern the assembly and spatial organization of the SMC-
819 mdol and SMC-mdol△*pilAB*. (A) Representative colony patterns from the pattern formation assays of
820 SMC-mdol and SMC-mdol△*pilAB*, as well as the individual-based simulations with the modified model
821 according to experimental parameters (denoted as 'Model') and the model with additional limited
822 resource, L (denoted as 'Model-sectors'; see Supplementary information S1 for detail about the
823 modifications of these models), across eight different initial substrate concentrations. (B) Analysis of
824 community composition of the experimental formed colonies, as well as the model predicted colonies
825 across eight kinds of initial substrate concentrations. The purple dashed line indicates the relative fraction
826 of 'Detoxifier' calculated from the PF2, while the blue dashed line indicates the relative fraction of
827 'Detoxifier' calculated from the PF3. We use adjusted R^2 to quantify the prediction power, where PF2

shows a power of 0.51 for the assembly of SMC-mdol and 0.76 for that of SMC-mdol△*pilAB*, while PF3 shows a power of 0.52 for the assembly of SMC-mdol and 0.78 for that of SMC-mdol△*pilAB*. (C-D) Analysis of spatial assortment experimental patterns (C) and the model predicted patterns (D) across eight different initial substrate concentrations. Note the absolute values of spatial assortment from the experiments and simulations are incomparable due to the difference between their scales (means experimental patterns containing more cells) and calculation methods (See Methods and Supplementary Information S1 sections for detail), but the trends of variation across the substrate concentrations are the same. For experiments, six replicates were performed for each condition, while for simulations, eight replicates were performed.

Figure 5 Substrate concentration governs the geometry of the 'bubble' structures inside the spatial patterns developed by SMC-mdol. (A) Workflow of the image analysis of the 'bubble' area. 'bubbles' formed by Detoxifier cells were segmented and analyzed to get its area size (mm^2). In the right graph, bubbles are color-coded based on their individual area size, with brighter colors indicating larger sizes. (B) Average number of the bubbles in the colony formed by SMC-mdol in different initial substrate concentration. (C) Average area size of the bubbles inside the colony formed by SMC-mdol in different initial substrate concentration. Images used here is same as Figure 4.

Figure 6 Type IV pili, but not flagella, are required for formation of the 'bubble' structures. (A) Images show that the colony patterning formed by the three synthetic communities in 'MDOL' scenario (supplying initial substrate salicylate as the sole carbon source) and 'Competition' scenario (supplying final product pyruvate as the sole carbon source). Typical morphology of the colony edges is zoomed in. Images were obtained after 120-h incubation. (B) Analysis of spatial assortment of the patterns formed in all conditions. As mentioned before, Assortment value closer to zero means the corresponding pattern

850 is more mixed. (C) Analysis of community composition of the colony patterns formed in all conditions.

851 Six replicates were performed for each condition. Different lower-case letters in (B) or (C) indicate

852 significant difference among these conditions at 0.01 level (unpaired, two-tailed, Student's t-test).

Figures

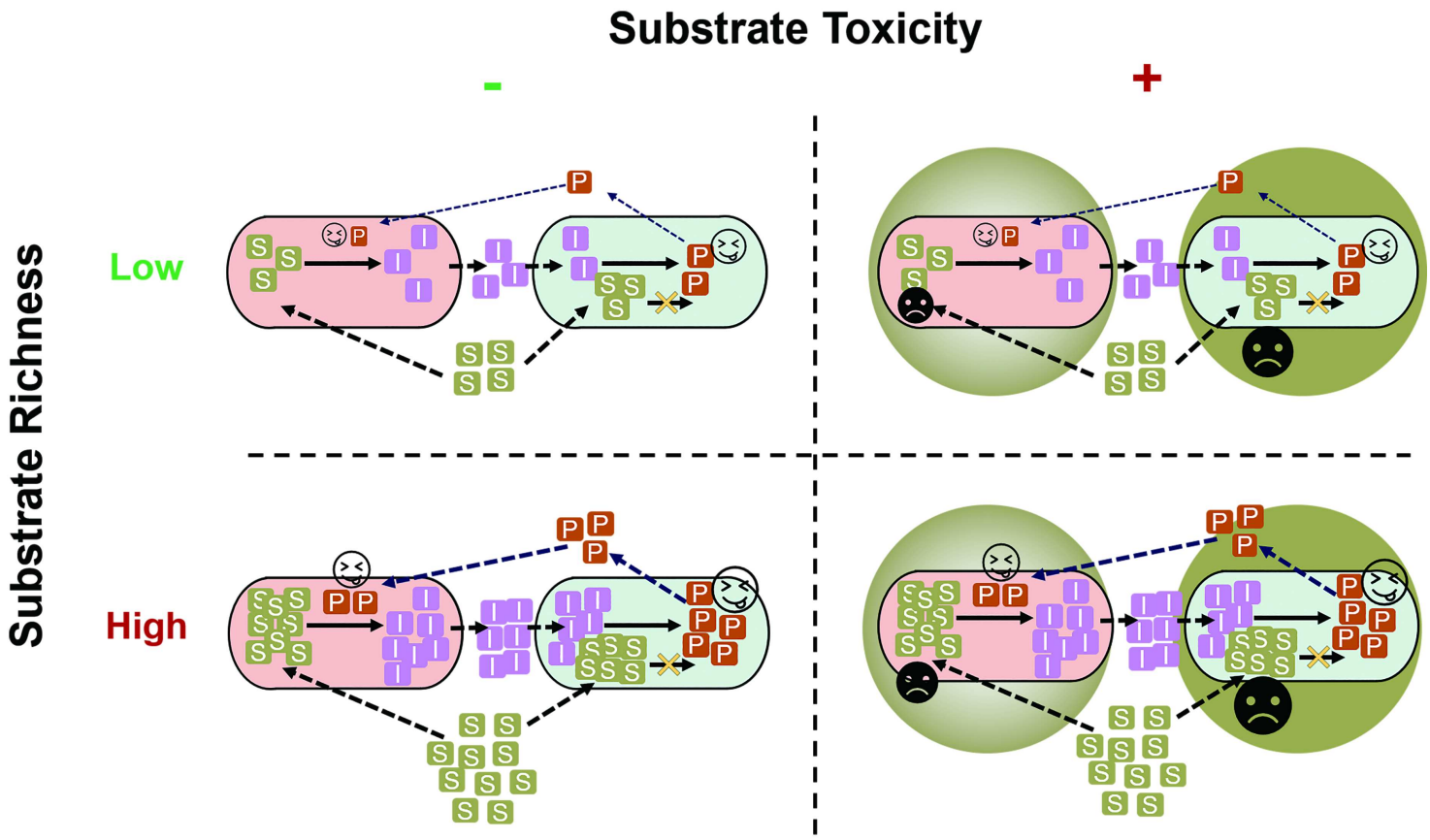

Figure 1

Hypotheses for how substrate concentration and toxicity govern the assembly of community involving MDOL. In a community degrading an organic compound through metabolic division of labor (MDOL), final product was assumed to be the sole resource and was synthesized by the strain performing the last step. Therefore, this strain will obtain more nutrients (denoted as bigger 'smiling face'), while the other strain has to collect product released from this population (denoted as smaller 'smiling face'). Thus, the last population was named 'Embezzler'. However, increasing the concentration of the substrate (vertical axis) improves the flux of the pathway, leading to higher final product leakiness, favoring the growth of the first population. Moreover, introducing substrate biotoxicity (horizontal axis) also favors the first population, because it performs conversion of this toxic substrate (denoted as smaller sad face), resulted in lower intracellular substrate concentration than the Embezzler cells (denoted as bigger sad face). Thus, the first population was named as 'Detoxifier'.

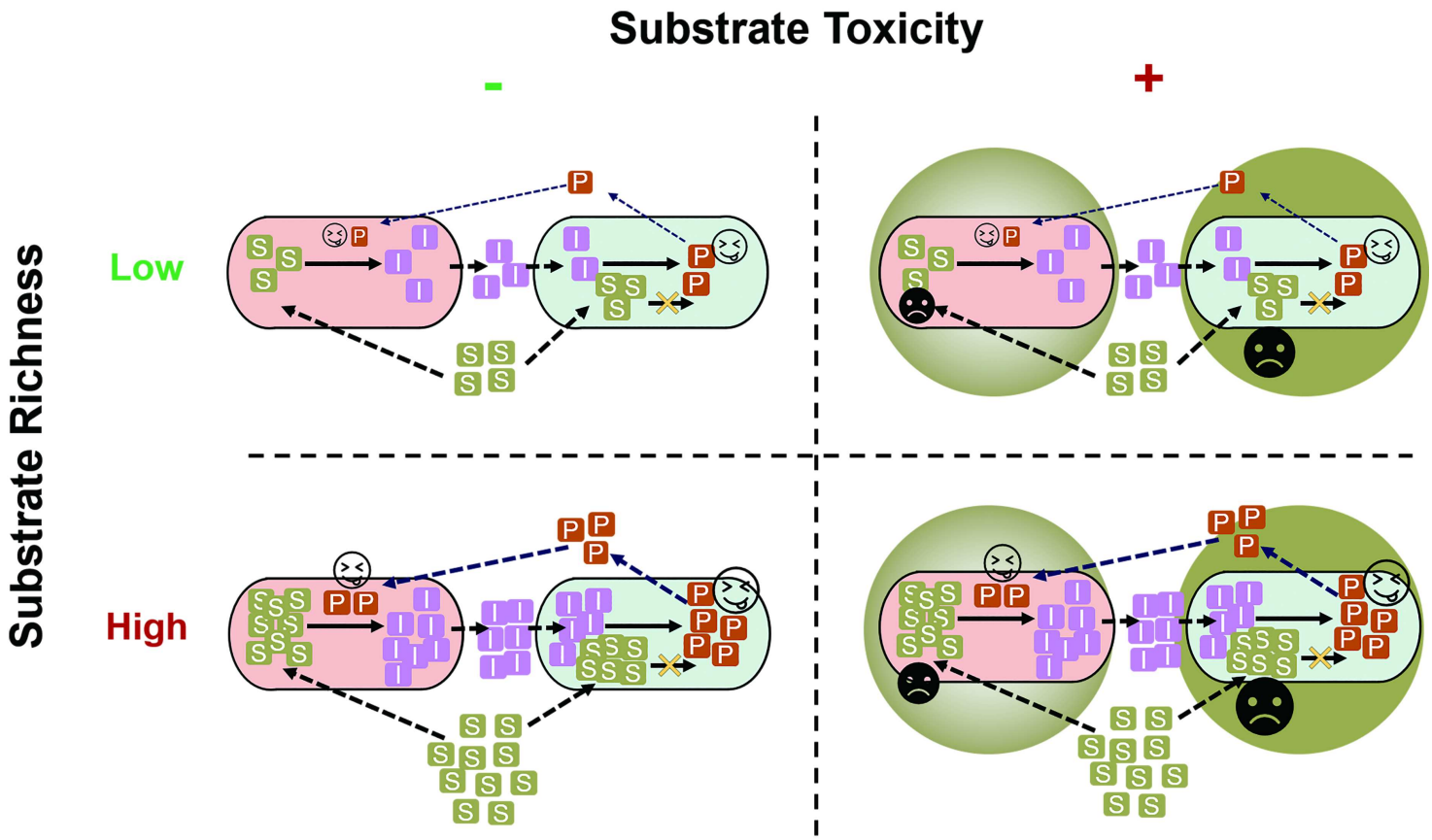

Figure 1

Hypotheses for how substrate concentration and toxicity govern the assembly of community involving MDOL. In a community degrading an organic compound through metabolic division of labor (MDOL), final product was assumed to be the sole resource and was synthesized by the strain performing the last step. Therefore, this strain will obtain more nutrients (denoted as bigger 'smiling face'), while the other strain has to collect product released from this population (denoted as smaller 'smiling face'). Thus, the last population was named 'Embezzler'. However, increasing the concentration of the substrate (vertical axis) improves the flux of the pathway, leading to higher final product leakiness, favoring the growth of the first population. Moreover, introducing substrate biotoxicity (horizontal axis) also favors the first population, because it performs conversion of this toxic substrate (denoted as smaller sad face), resulted in lower intracellular substrate concentration than the Embezzler cells (denoted as bigger sad face). Thus, the first population was named as 'Detoxifier'.

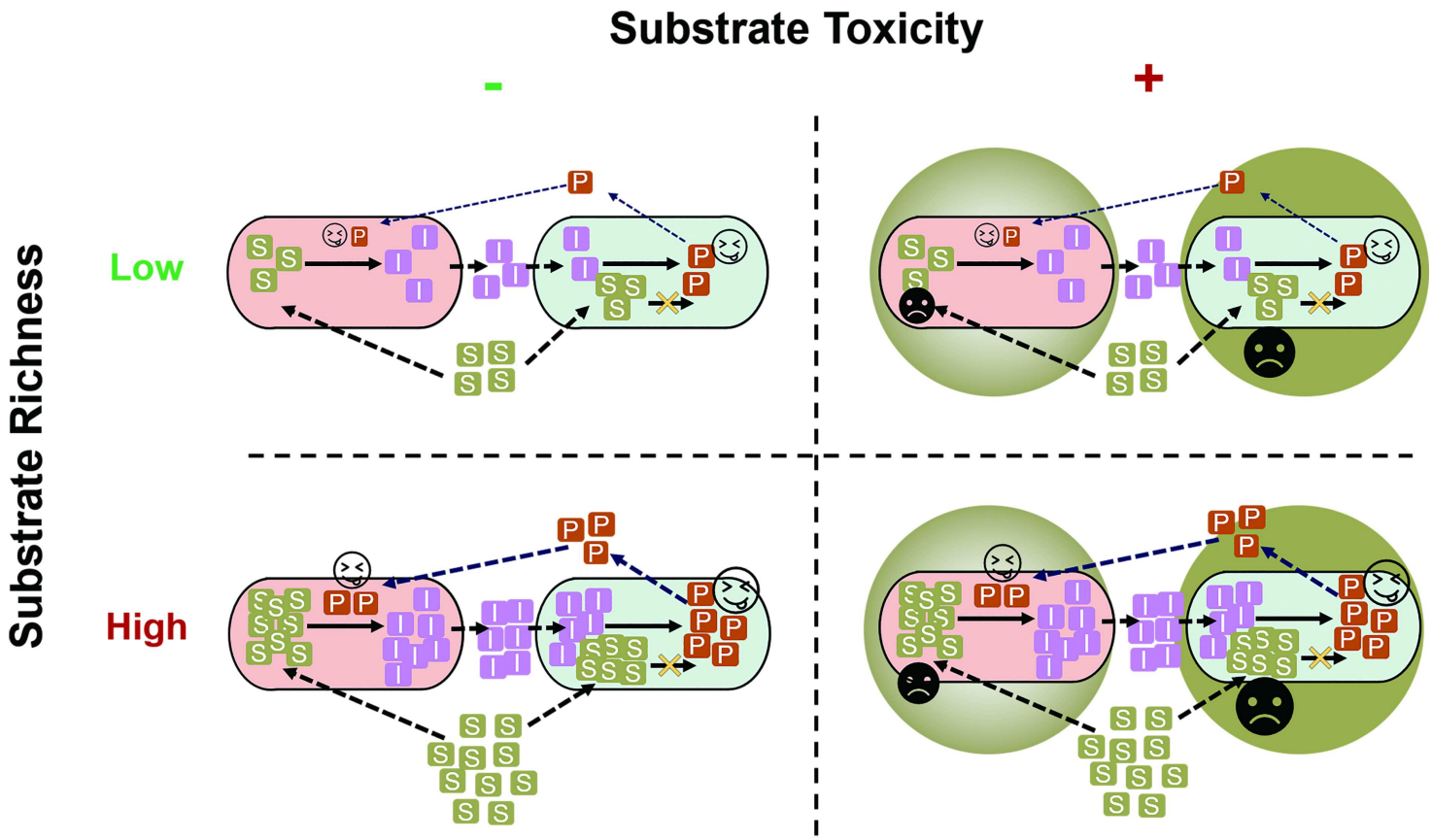

Figure 1

Hypotheses for how substrate concentration and toxicity govern the assembly of community involving MDOL. In a community degrading an organic compound through metabolic division of labor (MDOL), final product was assumed to be the sole resource and was synthesized by the strain performing the last step. Therefore, this strain will obtain more nutrients (denoted as bigger 'smiling face'), while the other strain has to collect product released from this population (denoted as smaller 'smiling face'). Thus, the last population was named 'Embezzler'. However, increasing the concentration of the substrate (vertical axis) improves the flux of the pathway, leading to higher final product leakiness, favoring the growth of the first population. Moreover, introducing substrate biotoxicity (horizontal axis) also favors the first population, because it performs conversion of this toxic substrate (denoted as smaller sad face), resulted in lower intracellular substrate concentration than the Embezzler cells (denoted as bigger sad face). Thus, the first population was named as 'Detoxifier'.

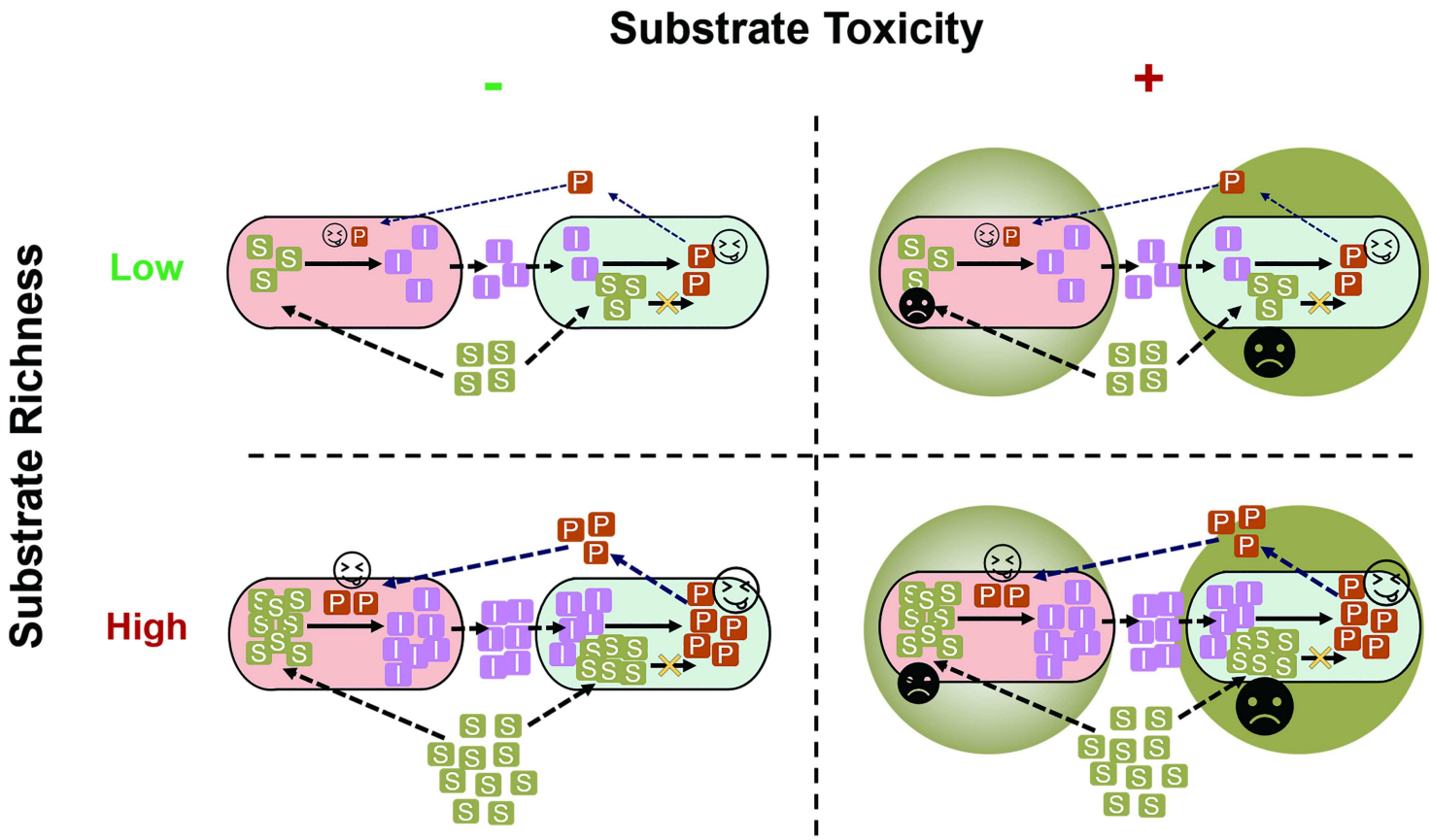

Figure 1

Hypotheses for how substrate concentration and toxicity govern the assembly of community involving MDOL. In a community degrading an organic compound through metabolic division of labor (MDOL), final product was assumed to be the sole resource and was synthesized by the strain performing the last step. Therefore, this strain will obtain more nutrients (denoted as bigger 'smiling face'), while the other strain has to collect product released from this population (denoted as smaller 'smiling face'). Thus, the last population was named 'Embezzler'. However, increasing the concentration of the substrate (vertical axis) improves the flux of the pathway, leading to higher final product leakiness, favoring the growth of the first population. Moreover, introducing substrate biotoxicity (horizontal axis) also favors the first population, because it performs conversion of this toxic substrate (denoted as smaller sad face), resulted in lower intracellular substrate concentration than the Embezzler cells (denoted as bigger sad face). Thus, the first population was named as 'Detoxifier'.

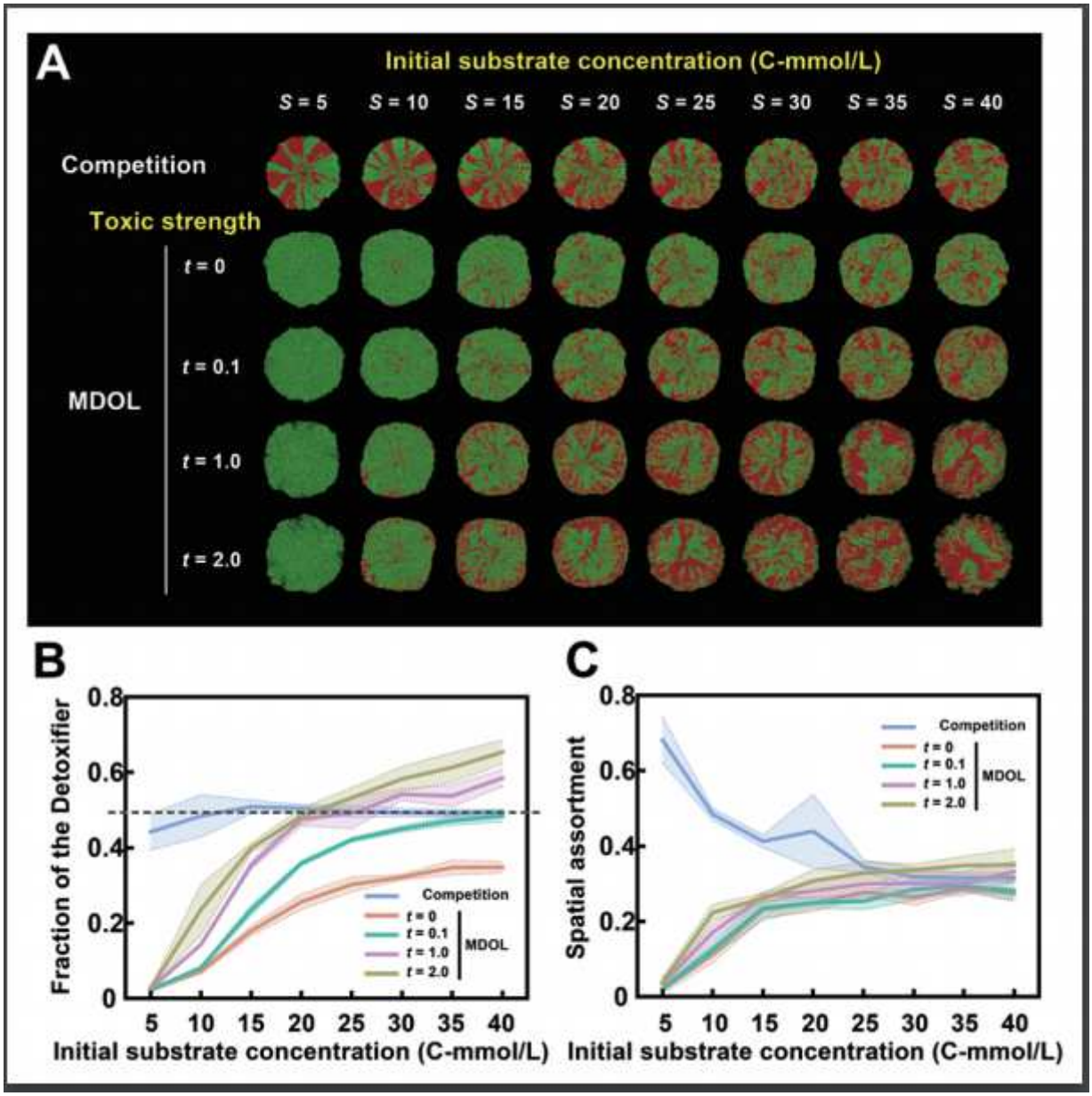

Figure 2

Individual-based modelling suggests that substrate concentration and toxicity govern the assembly and spatial organization of community involving MDOL. (A) Representative colony patterns from the simulations in 'MDOL' scenarios across eight kinds of initial substrate concentrations and four different toxic strength, as well as the patterns developed when two populations simply compete for P ('Competition' scenarios). (B) Analysis of community composition of these colonies. Plot shows the relationship between substrate concentration and toxicity with the relative fraction of Detoxifier cells. (C) Analysis of spatial assortment (intermixing level) of these colonies. Here, an assortment value of 0 means cells of the two populations is randomly distributed (i.e., a well-mixed pattern), while a value of 1 means the distribution of the two populations is totally segregated. Plot shows the relationship between substrate concentration and toxicity with the spatial assortment of the colonies. As described in Methods section, the closer that the assortment value to zero means the corresponding pattern is more mixed. All

the data were collected when the number of cells in the colony just reached 8100. Eight replicated simulations were performed for each condition.

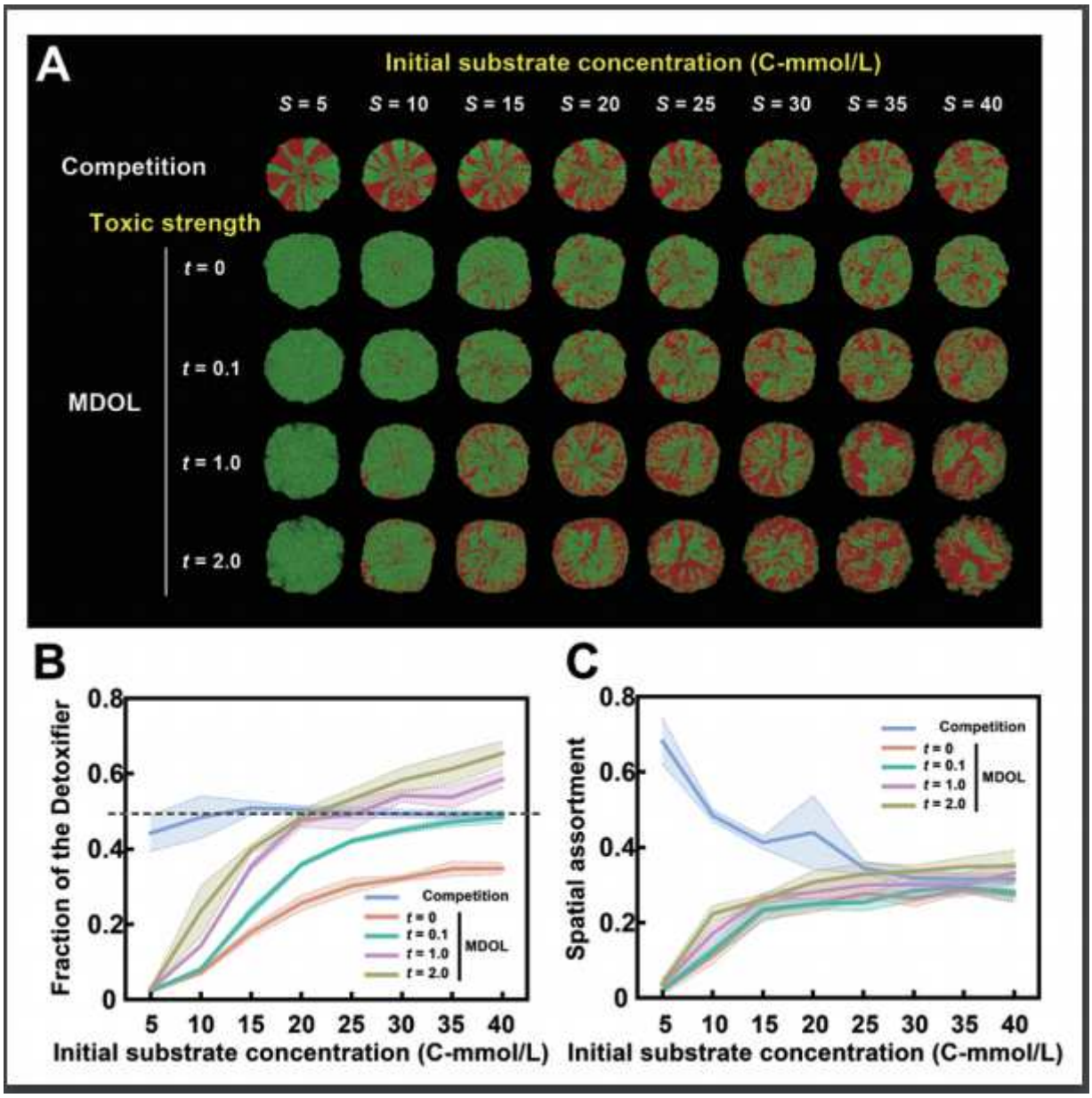

Figure 2

Individual-based modelling suggests that substrate concentration and toxicity govern the assembly and spatial organization of community involving MDOL. (A) Representative colony patterns from the simulations in 'MDOL' scenarios across eight kinds of initial substrate concentrations and four different toxic strength, as well as the patterns developed when two populations simply compete for P ('Competition' scenarios). (B) Analysis of community composition of these colonies. Plot shows the relationship between substrate concentration and toxicity with the relative fraction of Detoxifier cells. (C) Analysis of spatial assortment (intermixing level) of these colonies. Here, an assortment value of 0 means cells of the two populations is randomly distributed (i.e., a well-mixed pattern), while a value of 1 means the distribution of the two populations is totally segregated. Plot shows the relationship between substrate concentration and toxicity with the spatial assortment of the colonies. As described in Methods

section, the closer that the assortment value to zero means the corresponding pattern is more mixed. All the data were collected when the number of cells in the colony just reached 8100. Eight replicated simulations were performed for each condition.

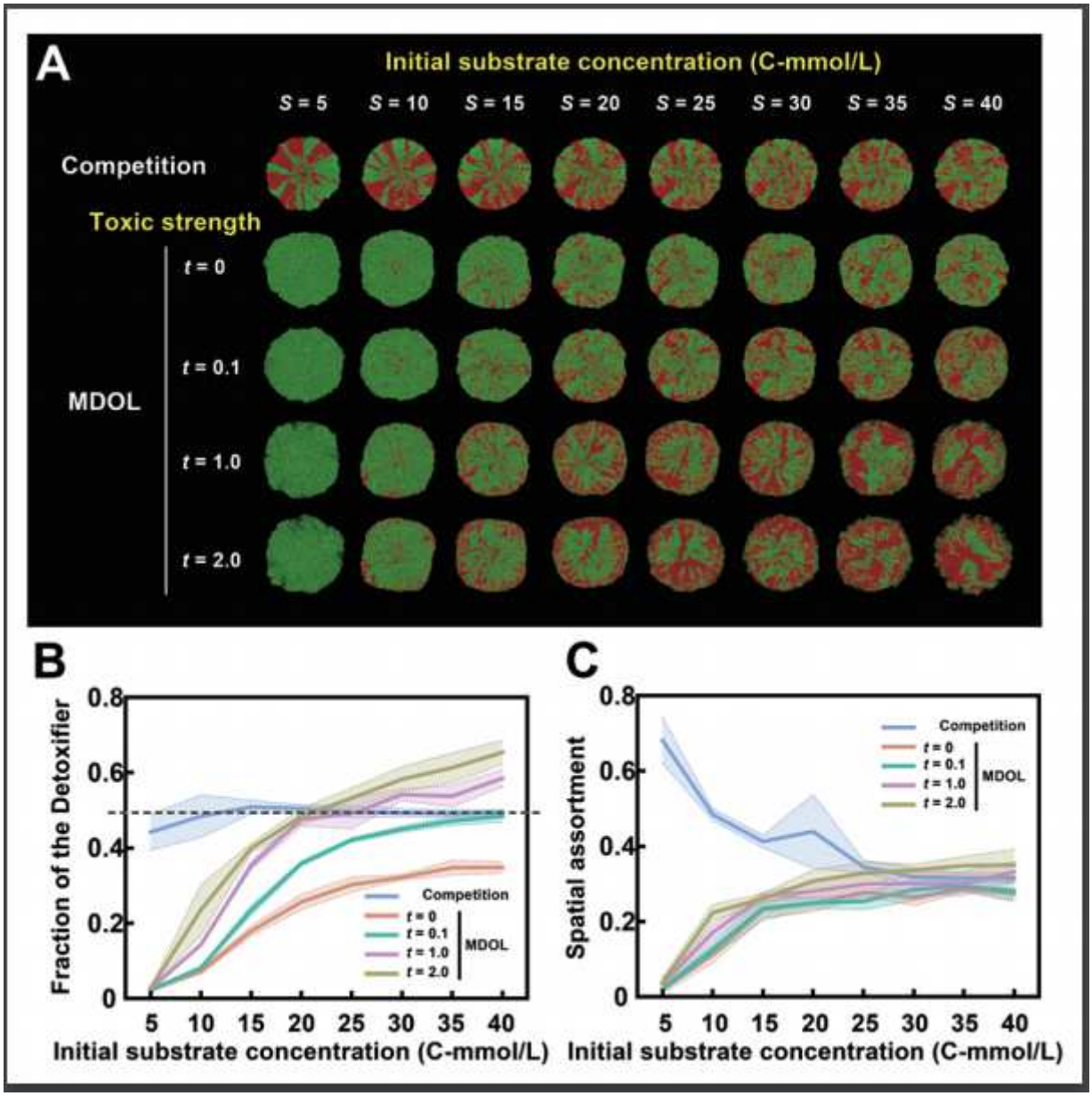

Figure 2

Individual-based modelling suggests that substrate concentration and toxicity govern the assembly and spatial organization of community involving MDOL. (A) Representative colony patterns from the simulations in 'MDOL' scenarios across eight kinds of initial substrate concentrations and four different toxic strength, as well as the patterns developed when two populations simply compete for P ('Competition' scenarios). (B) Analysis of community composition of these colonies. Plot shows the relationship between substrate concentration and toxicity with the relative fraction of Detoxifier cells. (C) Analysis of spatial assortment (intermixing level) of these colonies. Here, an assortment value of 0 means cells of the two populations is randomly distributed (i.e., a well-mixed pattern), while a value of 1 means the distribution of the two populations is totally segregated. Plot shows the relationship between

substrate concentration and toxicity with the spatial assortment of the colonies. As described in Methods section, the closer that the assortment value to zero means the corresponding pattern is more mixed. All the data were collected when the number of cells in the colony just reached 8100. Eight replicated simulations were performed for each condition.

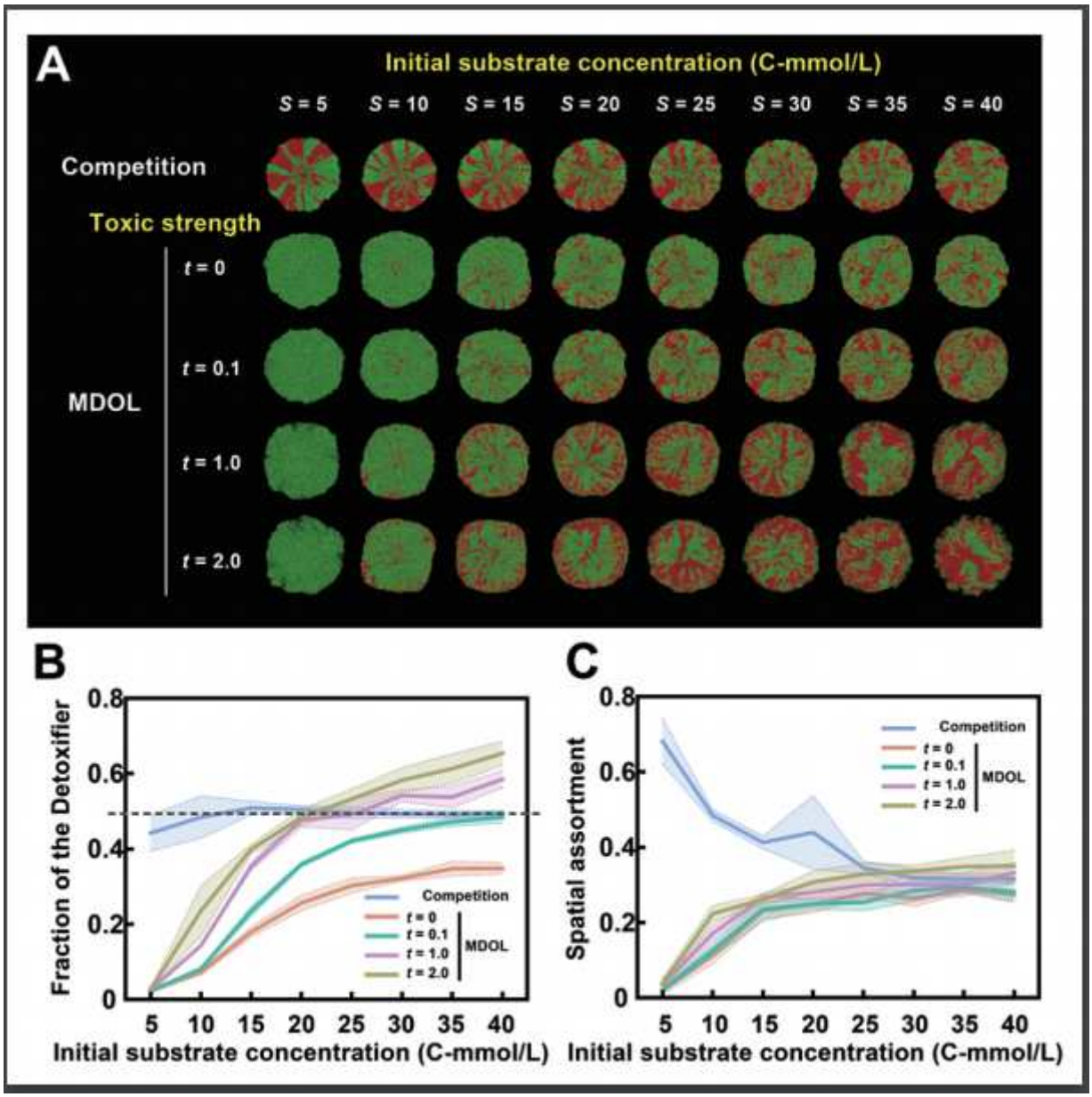

Figure 2

Individual-based modelling suggests that substrate concentration and toxicity govern the assembly and spatial organization of community involving MDOL. (A) Representative colony patterns from the simulations in 'MDOL' scenarios across eight kinds of initial substrate concentrations and four different toxic strength, as well as the patterns developed when two populations simply compete for P ('Competition' scenarios). (B) Analysis of community composition of these colonies. Plot shows the relationship between substrate concentration and toxicity with the relative fraction of Detoxifier cells. (C) Analysis of spatial assortment (intermixing level) of these colonies. Here, an assortment value of 0 means cells of the two populations is randomly distributed (i.e., a well-mixed pattern), while a value of 1

means the distribution of the two populations is totally segregated. Plot shows the relationship between substrate concentration and toxicity with the spatial assortment of the colonies. As described in Methods section, the closer that the assortment value to zero means the corresponding pattern is more mixed. All the data were collected when the number of cells in the colony just reached 8100. Eight replicated simulations were performed for each condition.

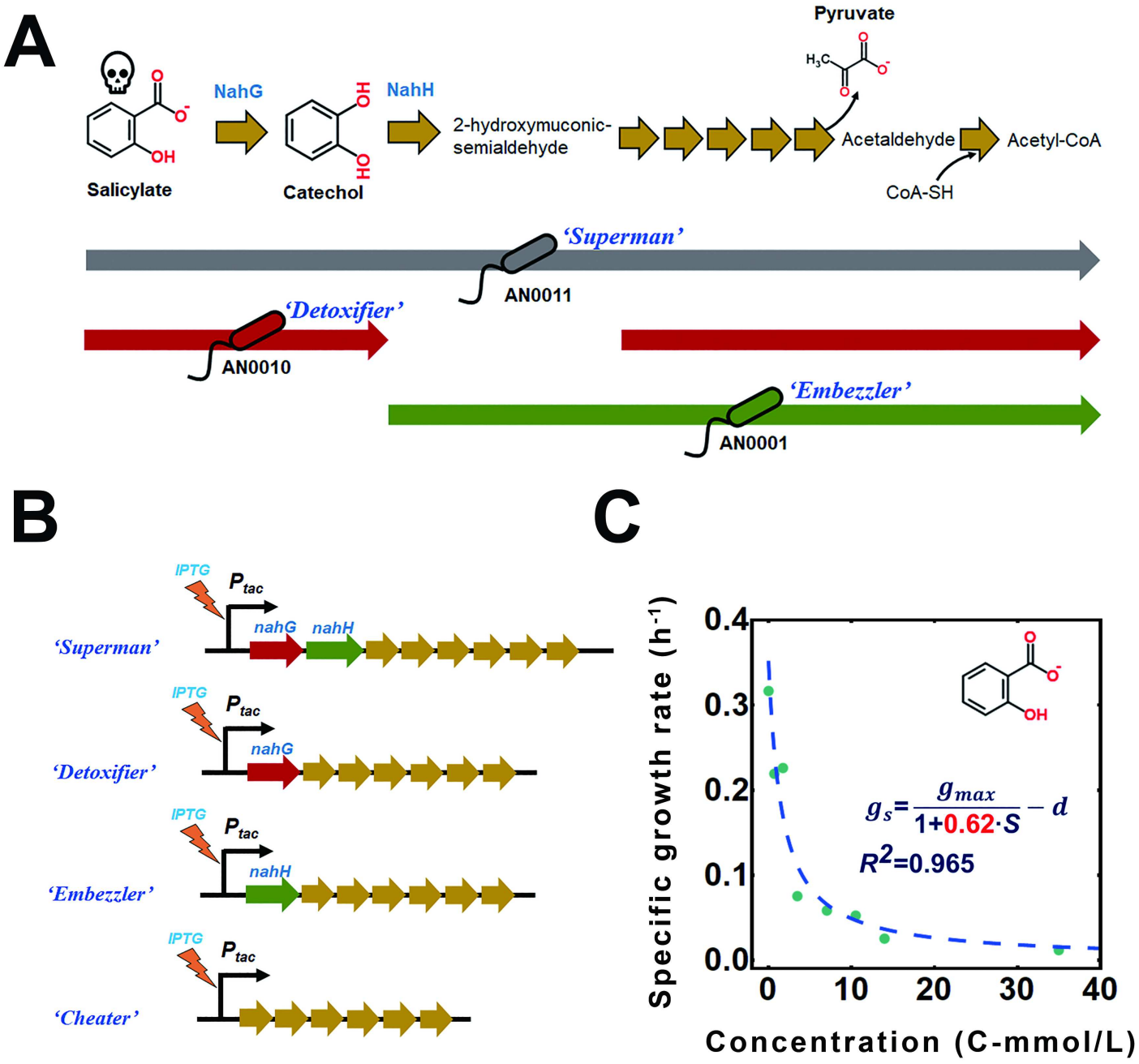

Figure 3

Design of the SMC-mdol. (A) Pathway of salicylate degradation in 'Superman' strain P. stutzeri AN0011, as well as partial pathways carried out by Detoxifier strain AN0010 and Embezzler strain AN0001. Skull marks that salicylate is toxic. (B) Diagram of operons responsible for the salicylate degradation, located in the chromosomes of AN0011, AN0010, AN0001 as well as a homologous mutant AN0000. (C)

Determination of the toxic strength of the substrate salicylate. We measured the growth rate of AN0000 using pyruvate, one of the end products, as the carbon source, and supplying different concentration of salicylate. The growth rates (g_s) were fitted with the corresponding salicylate concentration (S), using a formula involving maximum growth rate (g_max) and one-dimensional death rate (d), showing a hyperbolic toxic effect (See Methods section for detailed description).

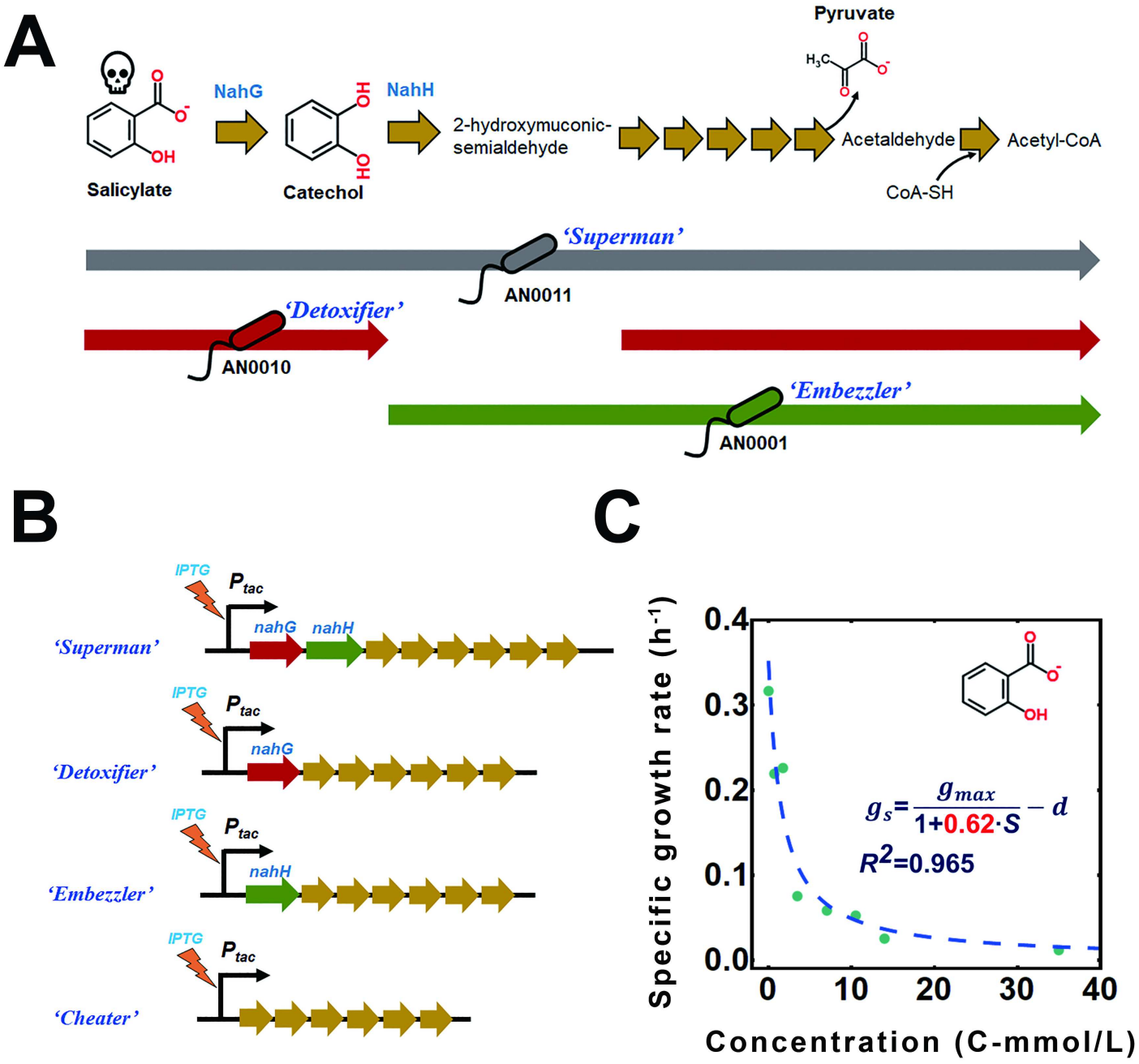

Figure 3

Design of the SMC-mdol. (A) Pathway of salicylate degradation in 'Superman' strain P. stutzeri AN0011, as well as partial pathways carried out by Detoxifier strain AN0010 and Embezzler strain AN0001. Skull marks that salicylate is toxic. (B) Diagram of operons responsible for the salicylate degradation, located in the chromosomes of AN0011, AN0010, AN0001 as well as a homologous mutant AN0000. (C)

Determination of the toxic strength of the substrate salicylate. We measured the growth rate of AN0000 using pyruvate, one of the end products, as the carbon source, and supplying different concentration of salicylate. The growth rates (g_s) were fitted with the corresponding salicylate concentration (S), using a formula involving maximum growth rate (g_max) and one-dimensional death rate (d), showing a hyperbolic toxic effect (See Methods section for detailed description).

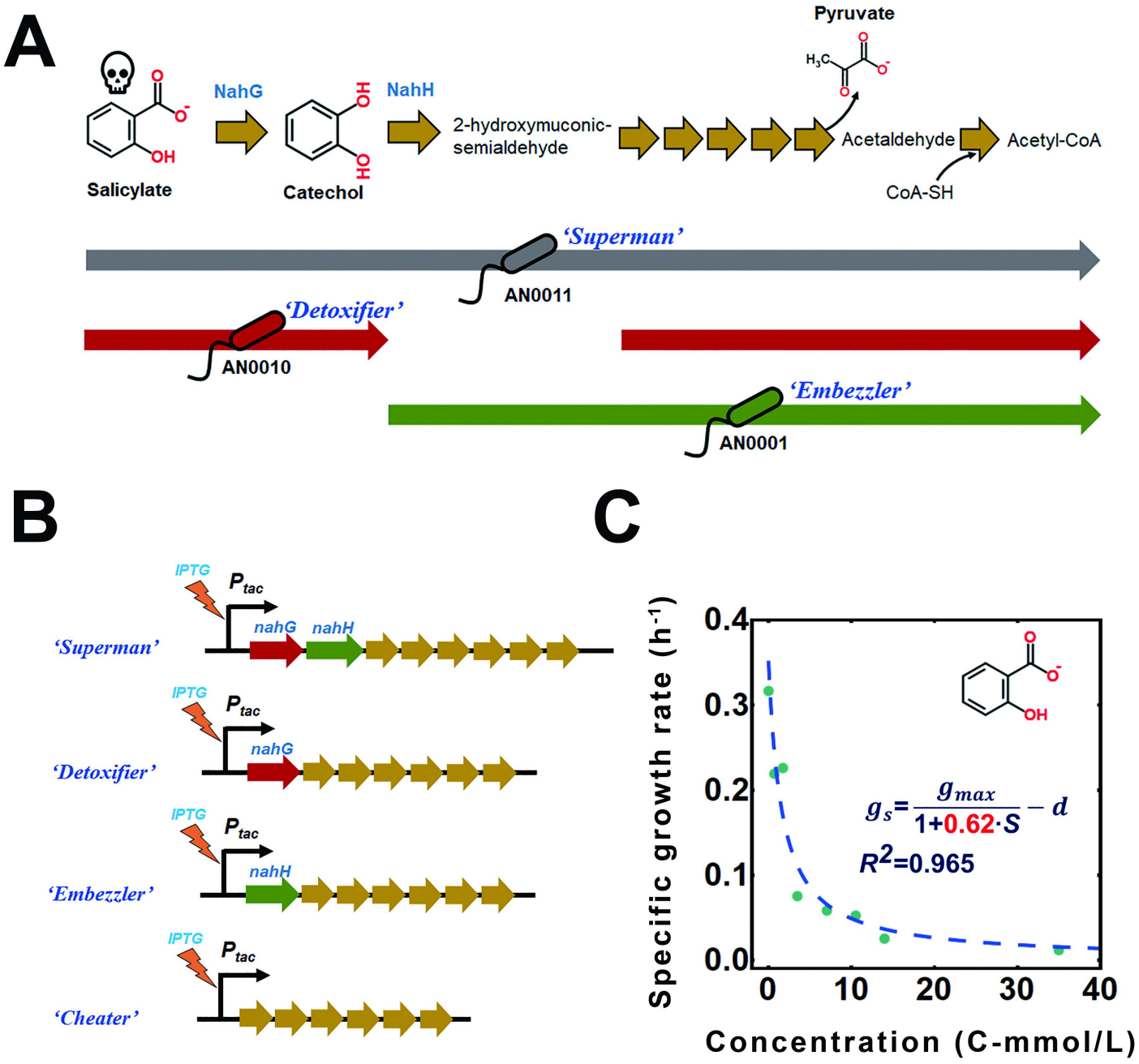

Figure 3

Design of the SMC-mdol. (A) Pathway of salicylate degradation in 'Superman' strain P. stutzeri AN0011, as well as partial pathways carried out by Detoxifier strain AN0010 and Embezzler strain AN0001. Skull marks that salicylate is toxic. (B) Diagram of operons responsible for the salicylate degradation, located in the chromosomes of AN0011, AN0010, AN0001 as well as a homologous mutant AN0000. (C)

Determination of the toxic strength of the substrate salicylate. We measured the growth rate of AN0000 using pyruvate, one of the end products, as the carbon source, and supplying different concentration of salicylate. The growth rates (g_s) were fitted with the corresponding salicylate concentration (S), using a formula involving maximum growth rate (g_max) and one-dimensional death rate (d), showing a hyperbolic toxic effect (See Methods section for detailed description).

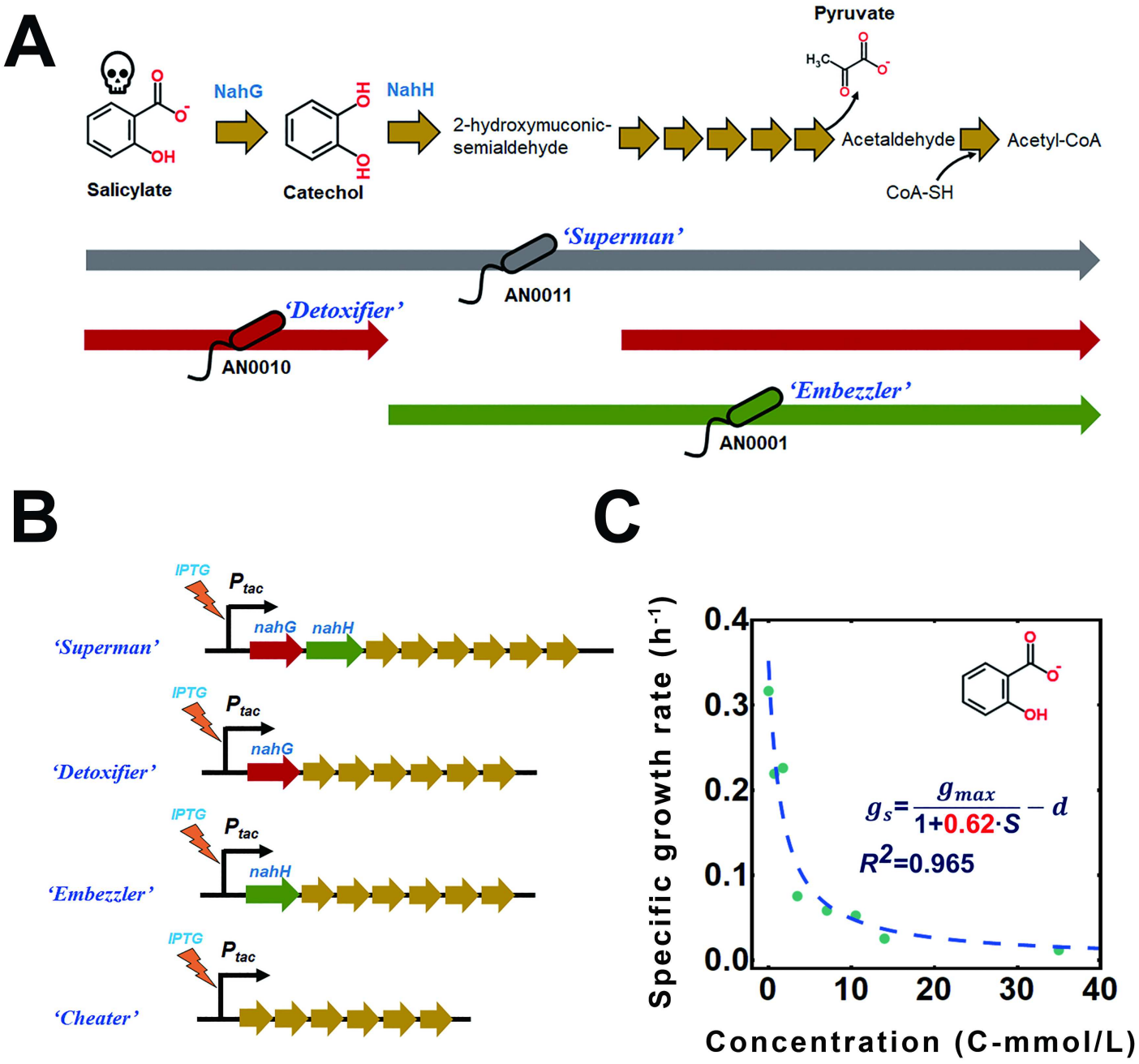

Figure 3

Design of the SMC-mdol. (A) Pathway of salicylate degradation in 'Superman' strain P. stutzeri AN0011, as well as partial pathways carried out by Detoxifier strain AN0010 and Embezzler strain AN0001. Skull marks that salicylate is toxic. (B) Diagram of operons responsible for the salicylate degradation, located in the chromosomes of AN0011, AN0010, AN0001 as well as a homologous mutant AN0000. (C)

Determination of the toxic strength of the substrate salicylate. We measured the growth rate of AN0000 using pyruvate, one of the end products, as the carbon source, and supplying different concentration of salicylate. The growth rates (g_s) were fitted with the corresponding salicylate concentration (S), using a formula involving maximum growth rate (g_max) and one-dimensional death rate (d), showing a hyperbolic toxic effect (See Methods section for detailed description).

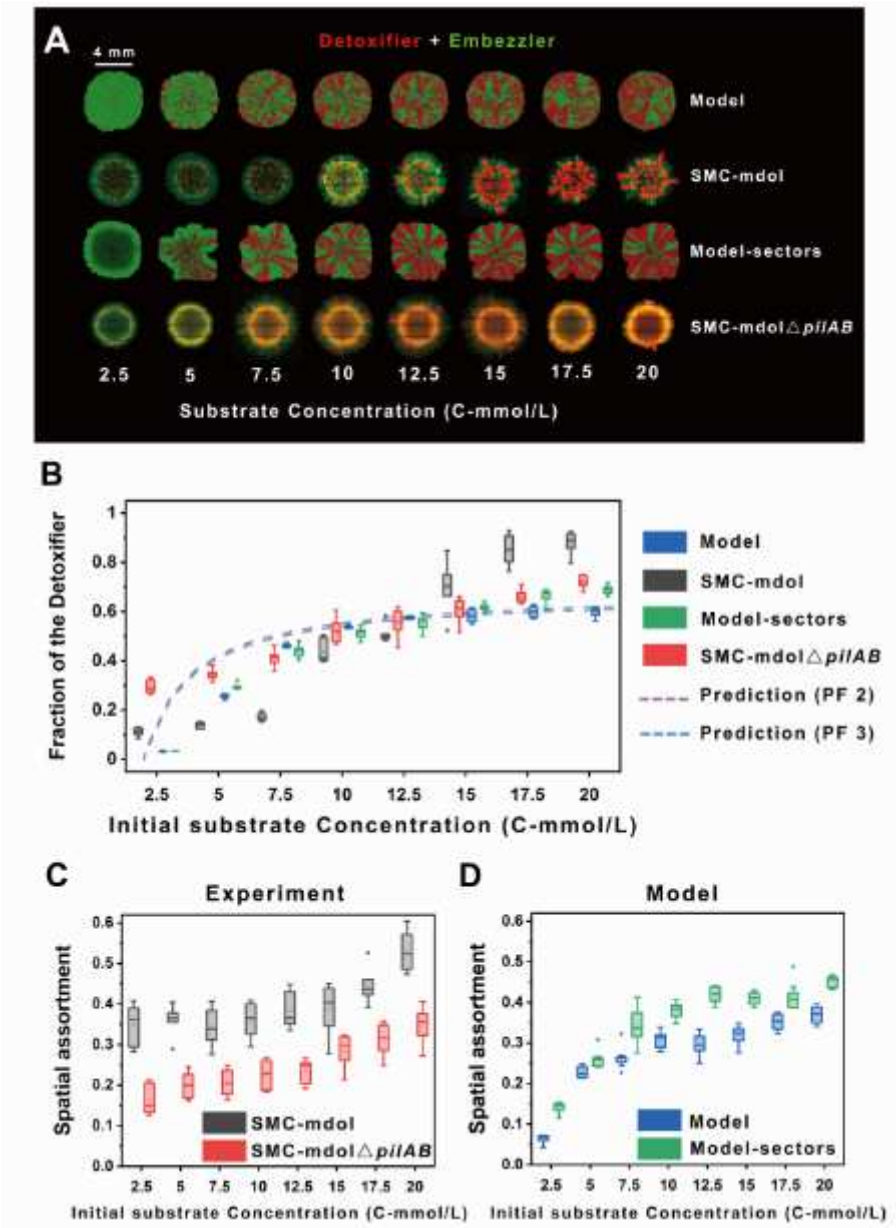

Figure 4

Substrate concentration and toxicity govern the assembly and spatial organization of the SMC-mdol and SMC-mdol□pilAB. (A) Representative colony patterns from the pattern formation assays of SMC-mdol and SMC-mdol□pilAB, as well as the individual-based simulations with the modified model according to experimental parameters (denoted as 'Model') and the model with additional limited resource, L (denoted as 'Model-sectors'; see Supplementary information S1 for detail about the modifications of these models), across eight different initial substrate concentrations. (B) Analysis of community composition of the experimental formed colonies, as well as the model predicted colonies across eight kinds of initial

substrate concentrations. The purple dashed line indicates the relative fraction of 'Detoxifier' calculated from the PF2, while the blue dashed line indicates the relative fraction of 'Detoxifier' calculated from the PF3. We use adjusted R2 to quantify the prediction power, where PF2 shows a power of 0.51 for the assembly of SMC-mdol and 0.76 for that of SMC-mdol△pilAB, while PF3 shows a power of 0.52 for the assembly of SMC-mdol and 0.78 for that of SMC-mdol△pilAB. (C-D) Analysis of spatial assortment experimental patterns (C) and the model predicted patterns (D) across eight different initial substrate concentrations. Note the absolute values of spatial assortment from the experiments and simulations are incomparable due to the difference between their scales (means experimental patterns containing more cells) and calculation methods (See Methods and Supplementary Information S1 sections for detail), but the trends of variation across the substrate concentrations are the same. For experiments, six replicates were performed for each condition, while for simulations, eight replicates were performed.

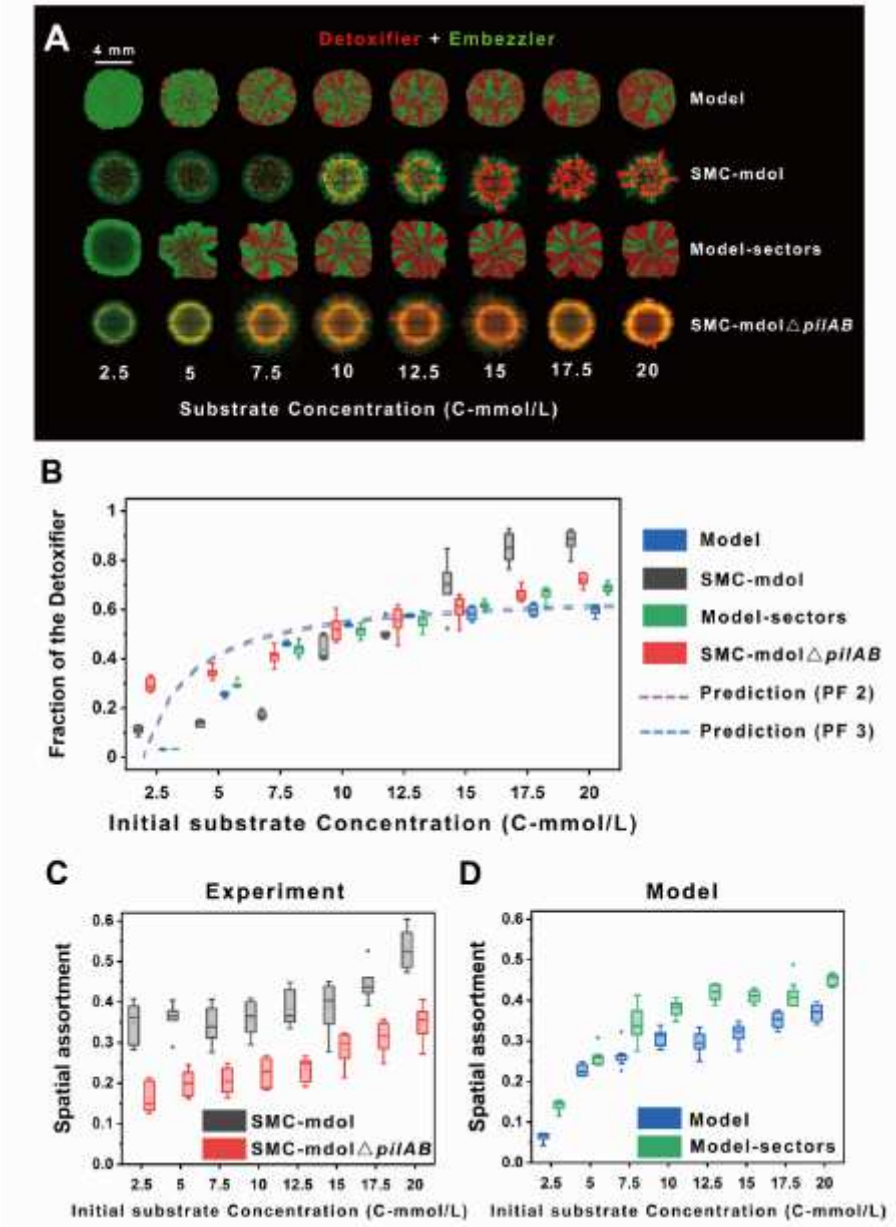

Figure 4

Substrate concentration and toxicity govern the assembly and spatial organization of the SMC-mdol and SMC-mdol□pilAB. (A) Representative colony patterns from the pattern formation assays of SMC-mdol and SMC-mdol□pilAB, as well as the individual-based simulations with the modified model according to experimental parameters (denoted as 'Model') and the model with additional limited resource, L (denoted as 'Model-sectors'; see Supplementary information S1 for detail about the modifications of these models), across eight different initial substrate concentrations. (B) Analysis of community composition of the experimental formed colonies, as well as the model predicted colonies across eight kinds of initial substrate concentrations. The purple dashed line indicates the relative fraction of 'Detoxifier' calculated from the PF2, while the blue dashed line indicates the relative fraction of 'Detoxifier' calculated from the PF3. We use adjusted R2 to quantify the prediction power, where PF2 shows a power of 0.51 for the assembly of SMC-mdol and 0.76 for that of SMC-mdol□pilAB, while PF3 shows a power of 0.52 for the assembly of SMC-mdol and 0.78 for that of SMC-mdol□pilAB. (C-D) Analysis of spatial assortment experimental patterns (C) and the model predicted patterns (D) across eight different initial substrate concentrations. Note the absolute values of spatial assortment from the experiments and simulations are incomparable due to the difference between their scales (means experimental patterns containing more cells) and calculation methods (See Methods and Supplementary Information S1 sections for detail), but the trends of variation across the substrate concentrations are the same. For experiments, six replicates were performed for each condition, while for simulations, eight replicates were performed.

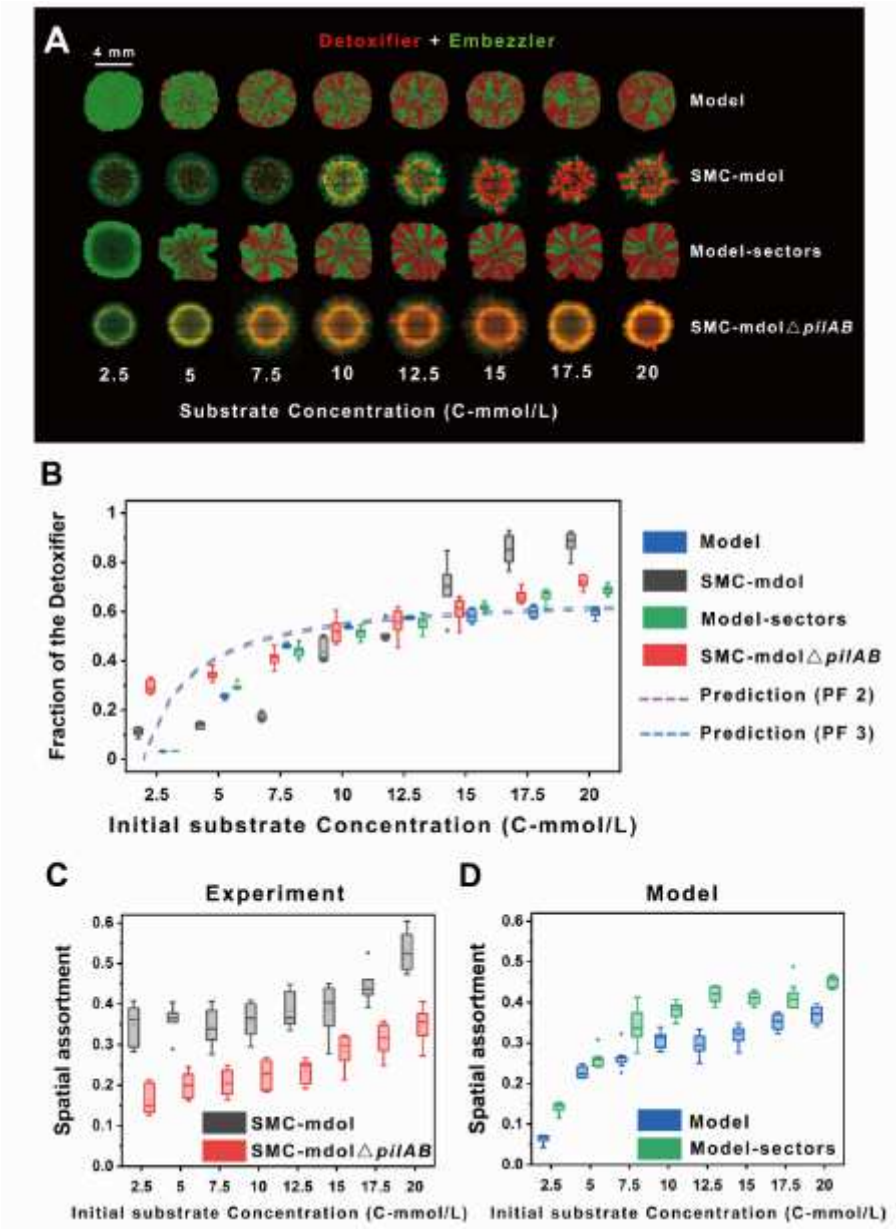

Figure 4

Substrate concentration and toxicity govern the assembly and spatial organization of the SMC-mdol and SMC-mdol□pilAB. (A) Representative colony patterns from the pattern formation assays of SMC-mdol and SMC-mdol□pilAB, as well as the individual-based simulations with the modified model according to experimental parameters (denoted as 'Model') and the model with additional limited resource, L (denoted as 'Model-sectors'; see Supplementary information S1 for detail about the modifications of these models), across eight different initial substrate concentrations. (B) Analysis of community composition of the experimental formed colonies, as well as the model predicted colonies across eight kinds of initial substrate concentrations. The purple dashed line indicates the relative fraction of 'Detoxifier' calculated from the PF2, while the blue dashed line indicates the relative fraction of 'Detoxifier' calculated from the PF3. We use adjusted R2 to quantify the prediction power, where PF2 shows a power of 0.51 for the assembly of SMC-mdol and 0.76 for that of SMC-mdol□pilAB, while PF3 shows a power of 0.52 for the assembly of SMC-mdol and 0.78 for that of SMC-mdol□pilAB. (C-D) Analysis of spatial assortment

experimental patterns (C) and the model predicted patterns (D) across eight different initial substrate concentrations. Note the absolute values of spatial assortment from the experiments and simulations are incomparable due to the difference between their scales (means experimental patterns containing more cells) and calculation methods (See Methods and Supplementary Information S1 sections for detail), but the trends of variation across the substrate concentrations are the same. For experiments, six replicates were performed for each condition, while for simulations, eight replicates were performed.

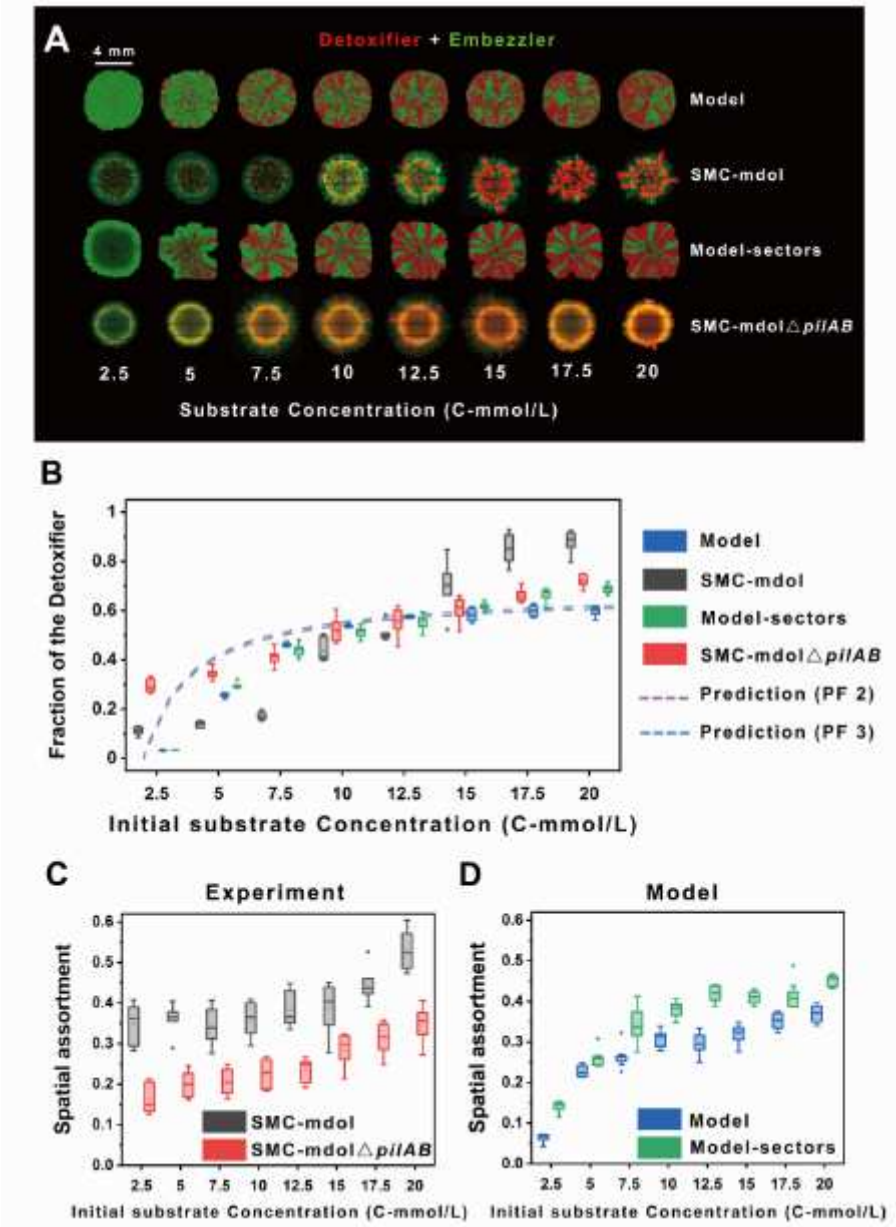

Figure 4

Substrate concentration and toxicity govern the assembly and spatial organization of the SMC-mdol and SMC-mdol□pilAB. (A) Representative colony patterns from the pattern formation assays of SMC-mdol and SMC-mdol□pilAB, as well as the individual-based simulations with the modified model according to experimental parameters (denoted as 'Model') and the model with additional limited resource, L (denoted as 'Model-sectors'; see Supplementary information S1 for detail about the modifications of these models), across eight different initial substrate concentrations. (B) Analysis of community composition

of the experimental formed colonies, as well as the model predicted colonies across eight kinds of initial substrate concentrations. The purple dashed line indicates the relative fraction of 'Detoxifier' calculated from the PF2, while the blue dashed line indicates the relative fraction of 'Detoxifier' calculated from the PF3. We use adjusted R2 to quantify the prediction power, where PF2 shows a power of 0.51 for the assembly of SMC-mdol and 0.76 for that of SMC-mdol□pilAB, while PF3 shows a power of 0.52 for the assembly of SMC-mdol and 0.78 for that of SMC-mdol□pilAB. (C-D) Analysis of spatial assortment experimental patterns (C) and the model predicted patterns (D) across eight different initial substrate concentrations. Note the absolute values of spatial assortment from the experiments and simulations are incomparable due to the difference between their scales (means experimental patterns containing more cells) and calculation methods (See Methods and Supplementary Information S1 sections for detail), but the trends of variation across the substrate concentrations are the same. For experiments, six replicates were performed for each condition, while for simulations, eight replicates were performed.

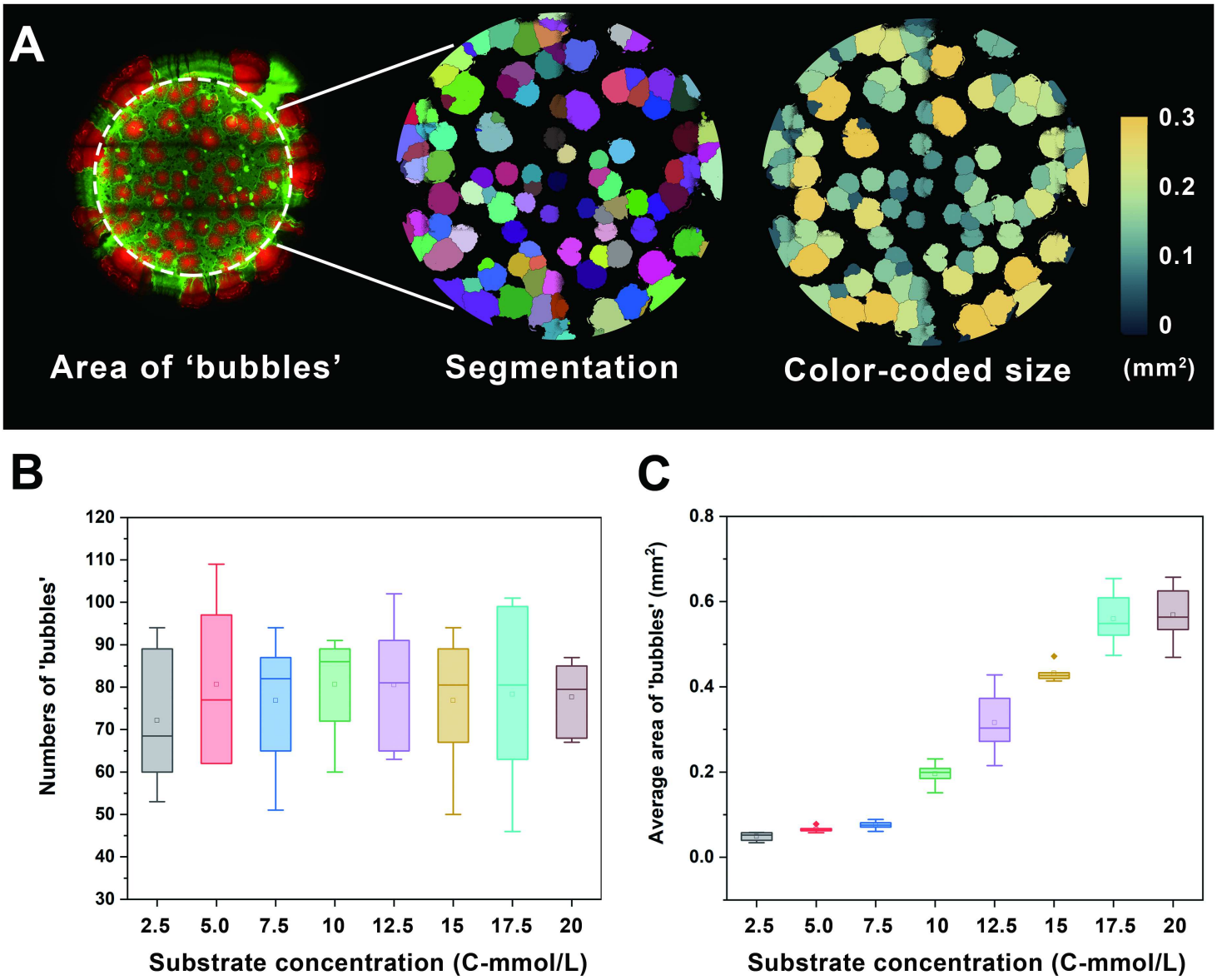

Figure 5

Substrate concentration governs the geometry of the ‘bubble’ structures inside the spatial patterns developed by SMC-mdol. (A) Workflow of the image analysis of the ‘bubble’ area. ‘bubbles’ formed by Detoxifier cells were segmented and analyzed to get its area size (mm2). In the right graph, bubbles are color-coded based on their individual area size, with brighter colors indicating larger sizes. (B) Average number of the bubbles in the colony formed by SMC-mdol in different initial substrate concentration. (C) Average area size of the bubbles inside the colony formed by SMC-mdol in different initial substrate concentration. Images used here is same as Figure 4.

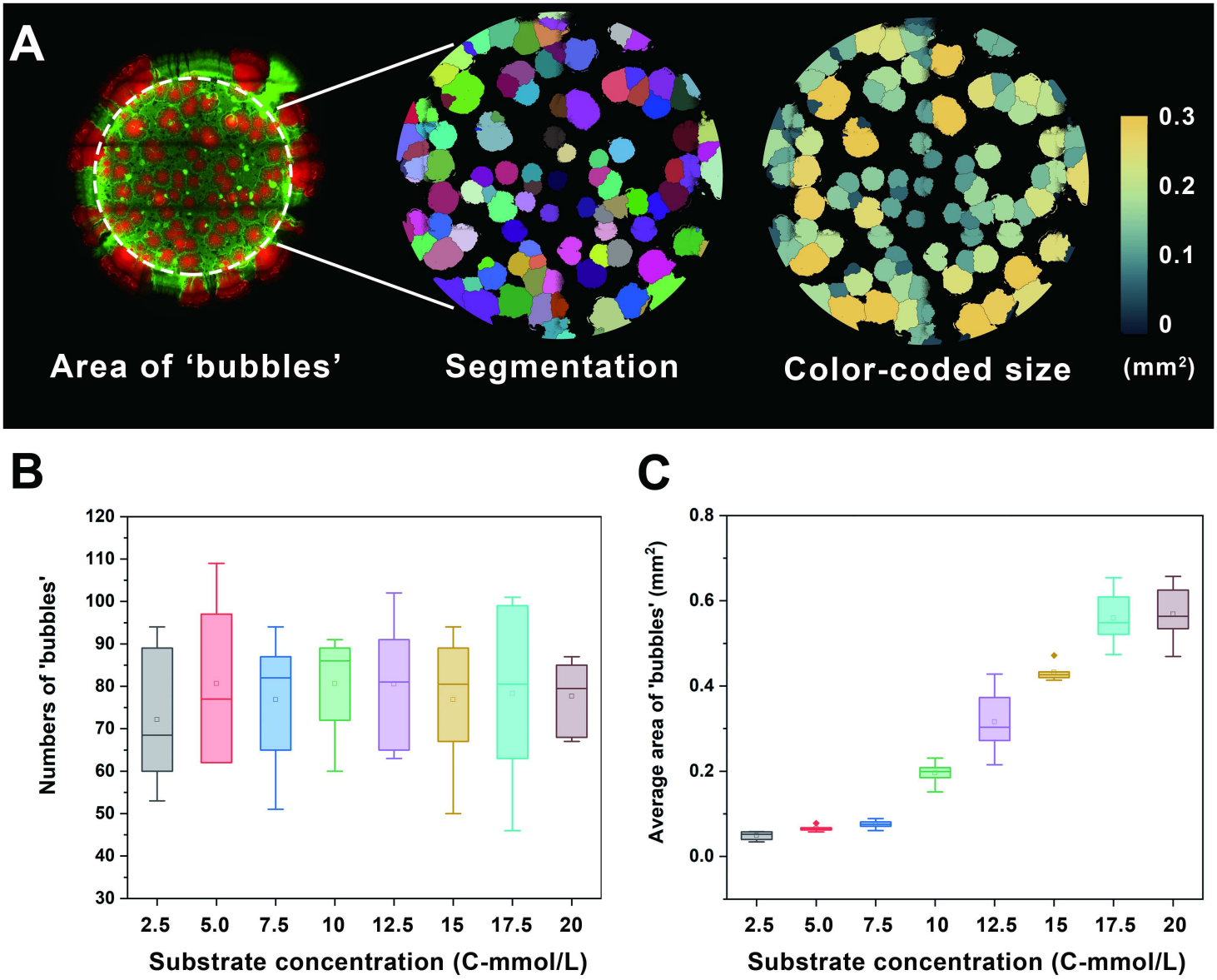

Figure 5

Substrate concentration governs the geometry of the ‘bubble’ structures inside the spatial patterns developed by SMC-mdol. (A) Workflow of the image analysis of the ‘bubble’ area. ‘bubbles’ formed by Detoxifier cells were segmented and analyzed to get its area size (mm2). In the right graph, bubbles are color-coded based on their individual area size, with brighter colors indicating larger sizes. (B) Average

number of the bubbles in the colony formed by SMC-mdol in different initial substrate concentration. (C) Average area size of the bubbles inside the colony formed by SMC-mdol in different initial substrate concentration. Images used here is same as Figure 4.

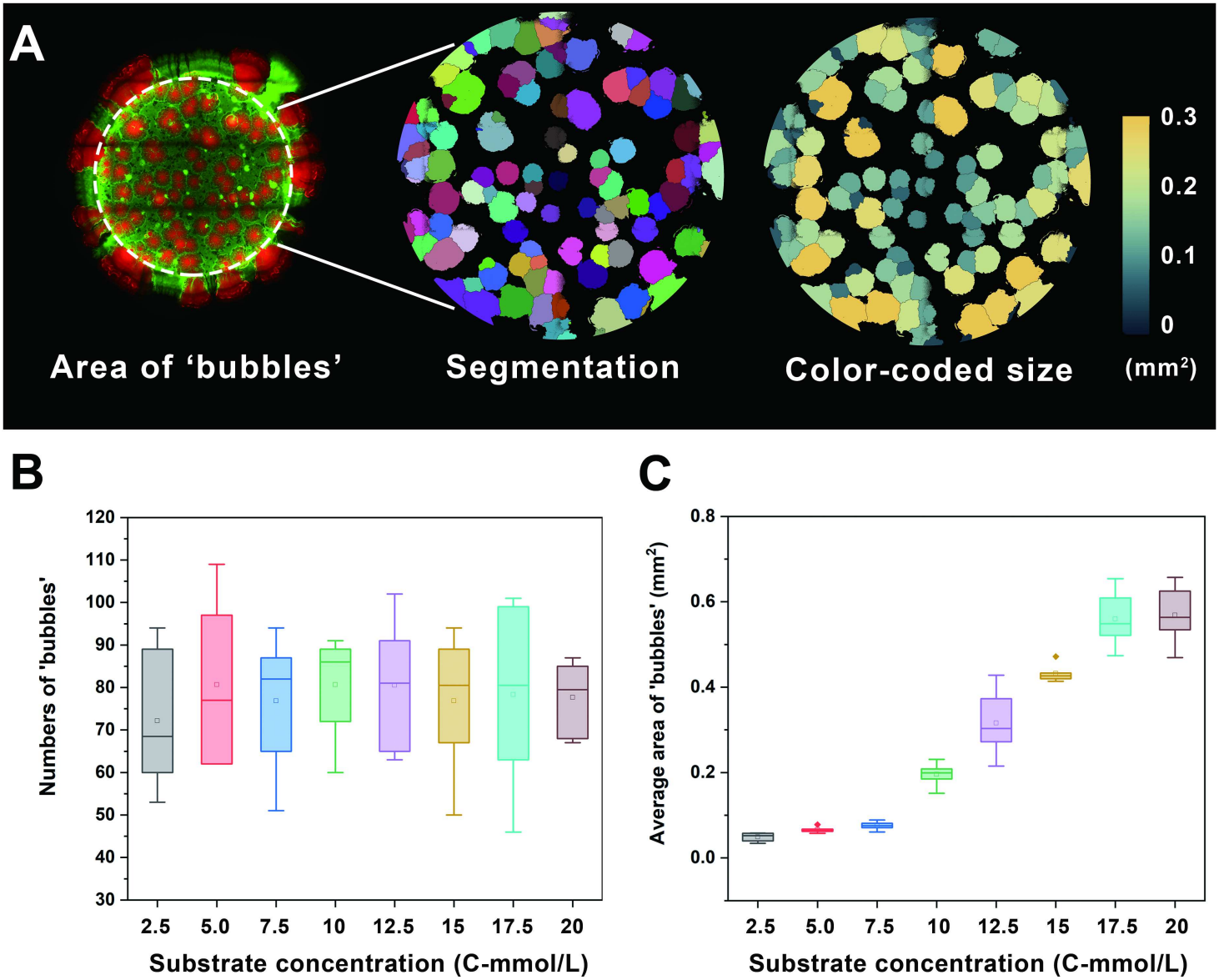

Figure 5

Substrate concentration governs the geometry of the 'bubble' structures inside the spatial patterns developed by SMC-mdol. (A) Workflow of the image analysis of the 'bubble' area. 'bubbles' formed by Detoxifier cells were segmented and analyzed to get its area size (mm2). In the right graph, bubbles are color-coded based on their individual area size, with brighter colors indicating larger sizes. (B) Average number of the bubbles in the colony formed by SMC-mdol in different initial substrate concentration. (C) Average area size of the bubbles inside the colony formed by SMC-mdol in different initial substrate concentration. Images used here is same as Figure 4.

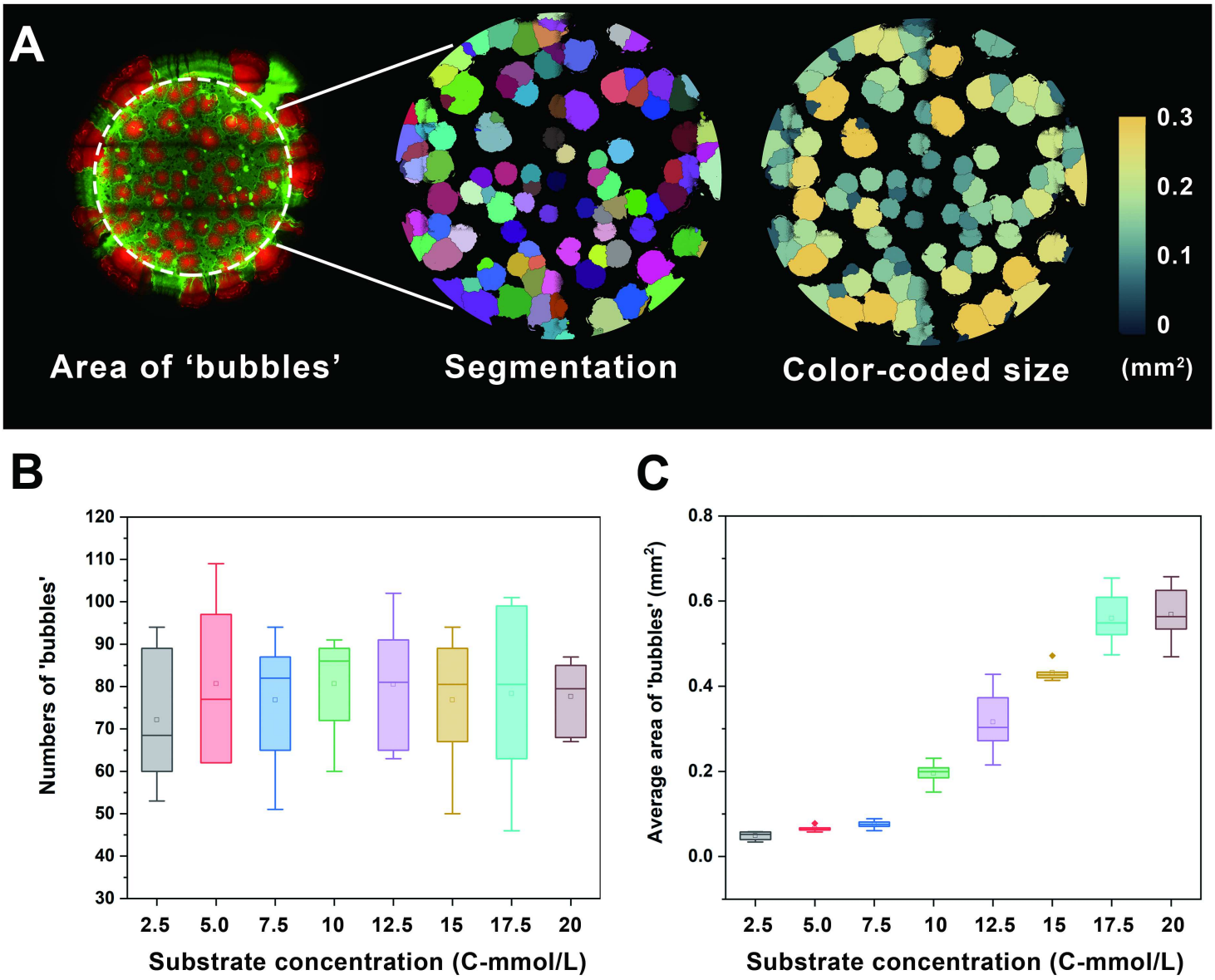

Figure 5

Substrate concentration governs the geometry of the 'bubble' structures inside the spatial patterns developed by SMC-mdol. (A) Workflow of the image analysis of the 'bubble' area. 'bubbles' formed by Detoxifier cells were segmented and analyzed to get its area size (mm2). In the right graph, bubbles are color-coded based on their individual area size, with brighter colors indicating larger sizes. (B) Average number of the bubbles in the colony formed by SMC-mdol in different initial substrate concentration. (C) Average area size of the bubbles inside the colony formed by SMC-mdol in different initial substrate concentration. Images used here is same as Figure 4.

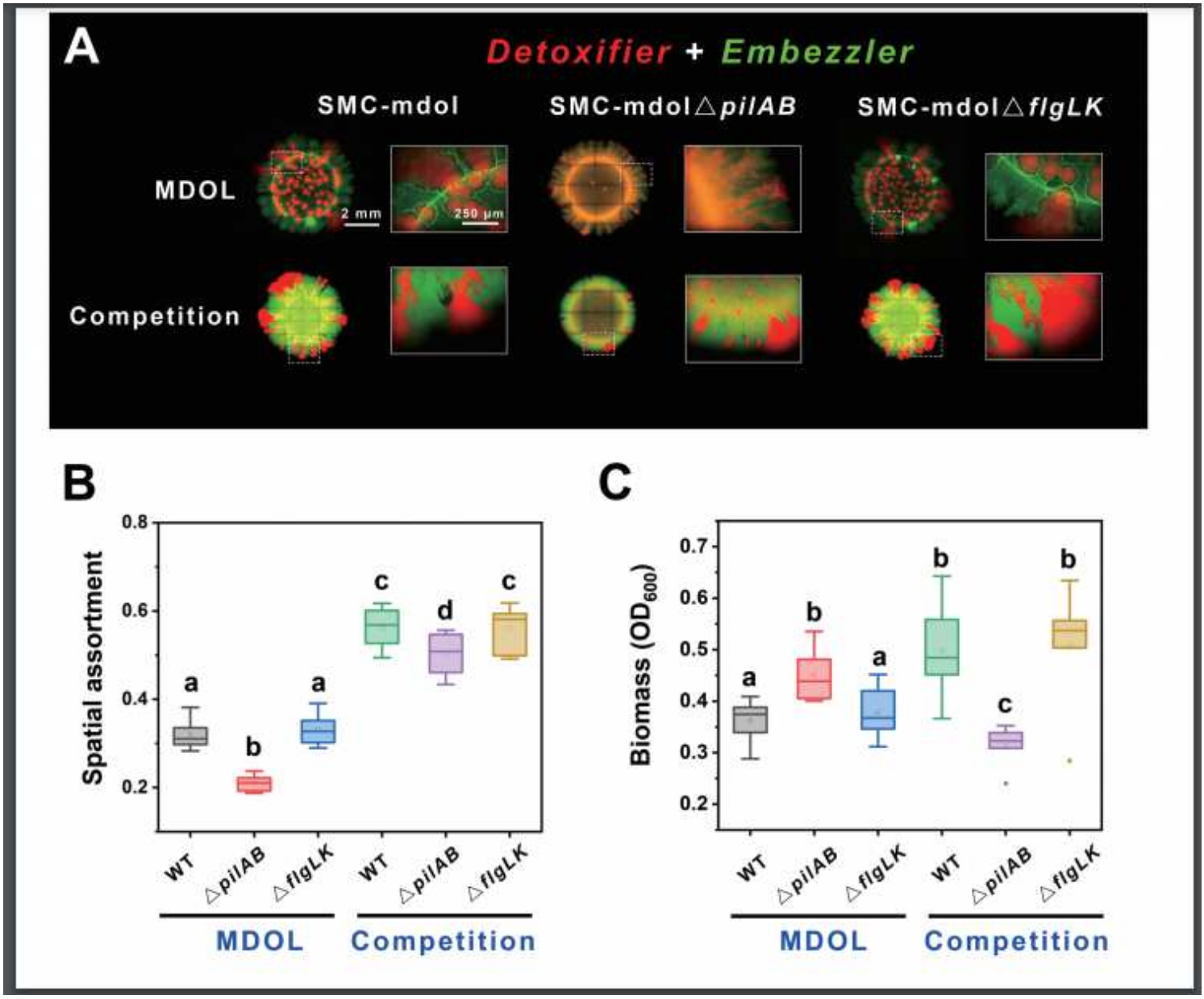

Figure 6

Type IV pili, but not flagella, are required for formation of the 'bubble' structures. (A) Images show that the colony patterning formed by the three synthetic communities in 'MDOL' scenario (supplying initial substrate salicylate as the sole carbon source) and 'Competition' scenario (supplying final product pyruvate as the sole carbon source). Typical morphology of the colony edges is zoomed in. Images were obtained after 120-h incubation. (B) Analysis of spatial assortment of the patterns formed in all conditions. As mentioned before, Assortment value closer to zero means the corresponding pattern is more mixed. (C) Analysis of community composition of the colony patterns formed in all conditions. Six replicates were performed for each condition. Different lower-case letters in (B) or (C) indicate significant difference among these conditions at 0.01 level (unpaired, two-tailed, Student's t-test).

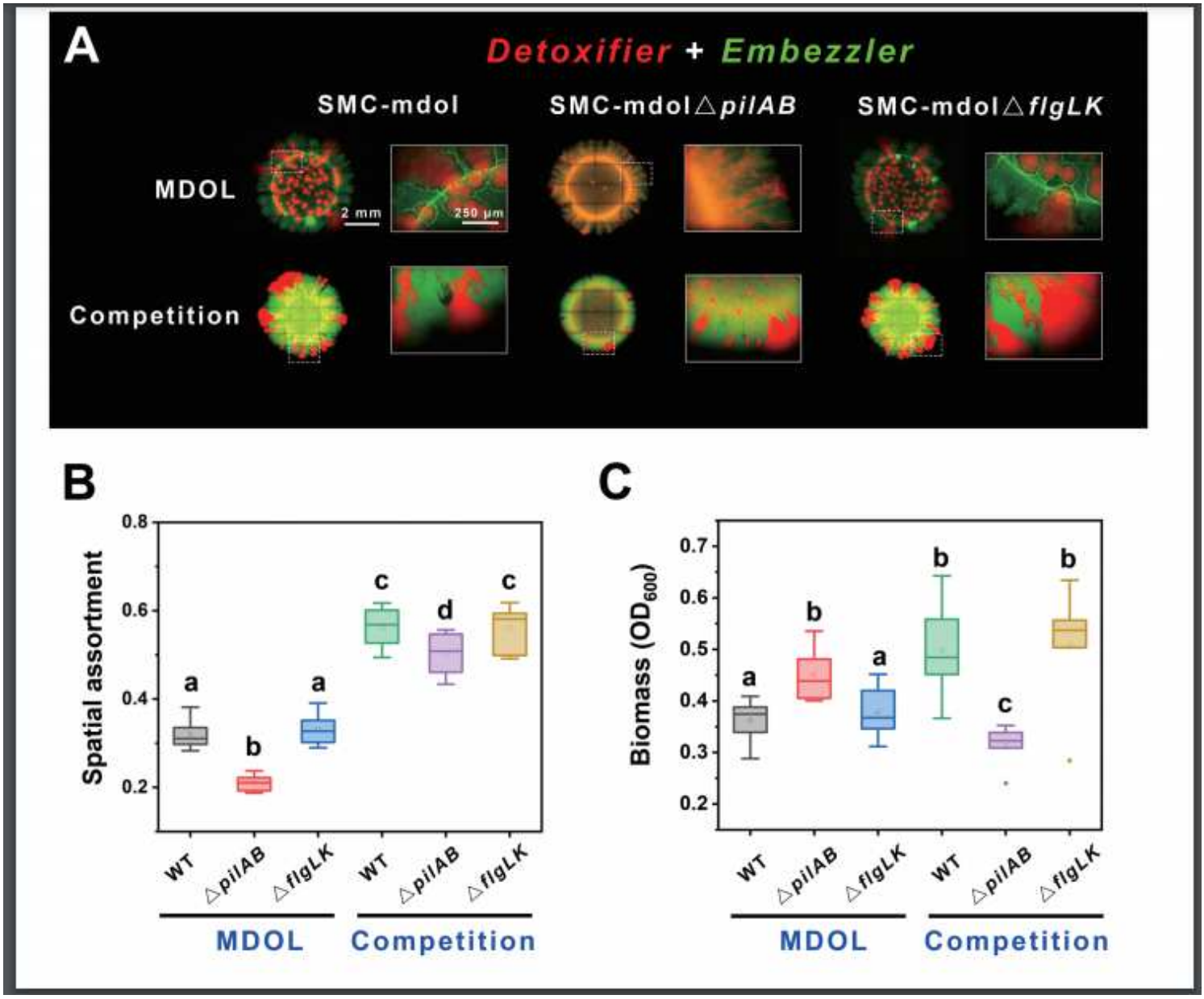

Figure 6

Type IV pili, but not flagella, are required for formation of the 'bubble' structures. (A) Images show that the colony patterning formed by the three synthetic communities in 'MDOL' scenario (supplying initial substrate salicylate as the sole carbon source) and 'Competition' scenario (supplying final product pyruvate as the sole carbon source). Typical morphology of the colony edges is zoomed in. Images were obtained after 120-h incubation. (B) Analysis of spatial assortment of the patterns formed in all conditions. As mentioned before, Assortment value closer to zero means the corresponding pattern is more mixed. (C) Analysis of community composition of the colony patterns formed in all conditions. Six replicates were performed for each condition. Different lower-case letters in (B) or (C) indicate significant difference among these conditions at 0.01 level (unpaired, two-tailed, Student's t-test).

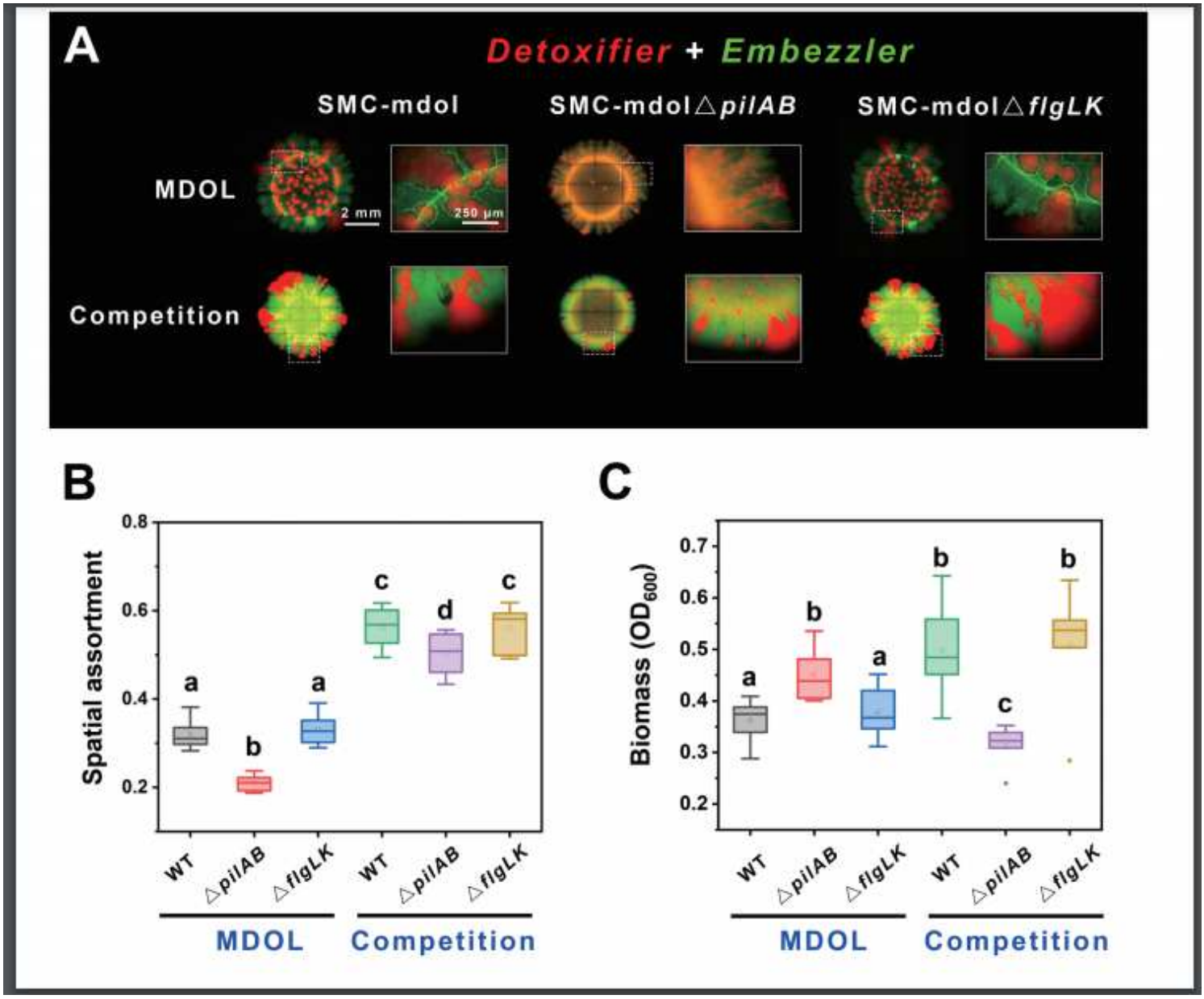

Figure 6

Type IV pili, but not flagella, are required for formation of the 'bubble' structures. (A) Images show that the colony patterning formed by the three synthetic communities in 'MDOL' scenario (supplying initial substrate salicylate as the sole carbon source) and 'Competition' scenario (supplying final product pyruvate as the sole carbon source). Typical morphology of the colony edges is zoomed in. Images were obtained after 120-h incubation. (B) Analysis of spatial assortment of the patterns formed in all conditions. As mentioned before, Assortment value closer to zero means the corresponding pattern is more mixed. (C) Analysis of community composition of the colony patterns formed in all conditions. Six replicates were performed for each condition. Different lower-case letters in (B) or (C) indicate significant difference among these conditions at 0.01 level (unpaired, two-tailed, Student's t-test).

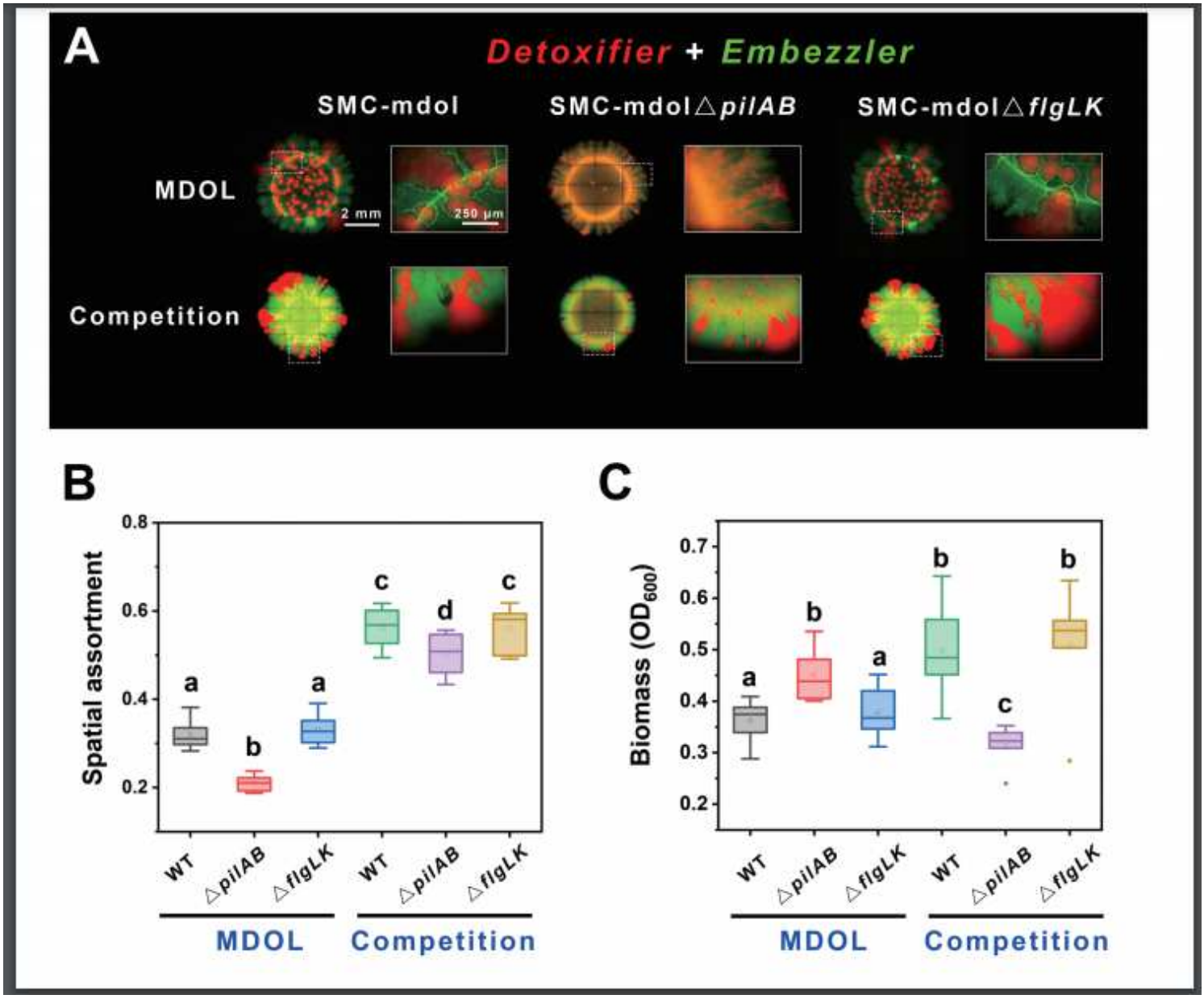

Figure 6

Type IV pili, but not flagella, are required for formation of the 'bubble' structures. (A) Images show that the colony patterning formed by the three synthetic communities in 'MDOL' scenario (supplying initial substrate salicylate as the sole carbon source) and 'Competition' scenario (supplying final product pyruvate as the sole carbon source). Typical morphology of the colony edges is zoomed in. Images were obtained after 120-h incubation. (B) Analysis of spatial assortment of the patterns formed in all conditions. As mentioned before, Assortment value closer to zero means the corresponding pattern is more mixed. (C) Analysis of community composition of the colony patterns formed in all conditions. Six replicates were performed for each condition. Different lower-case letters in (B) or (C) indicate significant difference among these conditions at 0.01 level (unpaired, two-tailed, Student's t-test).

Supplementary Files

This is a list of supplementary files associated with this preprint. Click to download.

- Supplementaryvideo1.avi
- Supplementaryvideo1.avi
- Supplementaryvideo1.avi
- Supplementaryvideo1.avi
- Supplementaryvideo2.avi
- Supplementaryvideo2.avi
- Supplementaryvideo2.avi
- Supplementaryvideo2.avi
- Supplementaryvideo3.avi
- Supplementaryvideo3.avi
- Supplementaryvideo3.avi
- Supplementaryvideo3.avi
- Supplementaryvideo4.avi
- Supplementaryvideo4.avi
- Supplementaryvideo4.avi
- Supplementaryvideo4.avi
- SupplementaryInformation20201118.docx
- SupplementaryInformation20201118.docx
- SupplementaryInformation20201118.docx
- SupplementaryInformation20201118.docx
- SupplementaryFigure1.tif
- SupplementaryFigure1.tif
- SupplementaryFigure1.tif
- SupplementaryFigure1.tif
- SupplementaryFigure2.tif
- SupplementaryFigure2.tif
- SupplementaryFigure2.tif
- SupplementaryFigure2.tif
- SupplementaryFigure3.tif
- SupplementaryFigure3.tif
- SupplementaryFigure3.tif
- SupplementaryFigure3.tif
- SupplementaryFigure4.tif

- SupplementaryFigure4.tif
- SupplementaryFigure4.tif
- SupplementaryFigure4.tif
- SupplementaryFigure5.tif
- SupplementaryFigure5.tif
- SupplementaryFigure5.tif
- SupplementaryFigure5.tif
- SupplementaryFigure6.tif
- SupplementaryFigure6.tif
- SupplementaryFigure6.tif
- SupplementaryFigure6.tif
- SupplementaryFigure7.tif
- SupplementaryFigure7.tif
- SupplementaryFigure7.tif
- SupplementaryFigure7.tif
- SupplementaryFigure8.tif
- SupplementaryFigure8.tif
- SupplementaryFigure8.tif
- SupplementaryFigure8.tif
- SupplementaryFigure9.tif
- SupplementaryFigure9.tif
- SupplementaryFigure9.tif
- SupplementaryFigure9.tif
- SupplementaryFigure10.tif
- SupplementaryFigure10.tif
- SupplementaryFigure10.tif
- SupplementaryFigure10.tif
- SupplementaryFigure11.tif
- SupplementaryFigure11.tif
- SupplementaryFigure11.tif
- SupplementaryFigure11.tif
- SupplementaryFigure12.tif
- SupplementaryFigure12.tif
- SupplementaryFigure12.tif

- SupplementaryFigure12.tif